1. Title Page

Murine CMV infection unmasks macrophage-driven inflammatory cardiomyopathy in *Pkp2*, but not in *Ttn* mutant mice

Alexandra Cirnu, MSc[1,#], Tatjana Williams, PhD[1,#], Mike Nörpel, MD[1], Julian Kammerer[1], Svenja Kannt[1], Mairin Heil, MSc[1], Laura Kimmel, MSc[1], Anahi-Paula Arias-Loza, PhD[2], Manivel Lhoda, PhD[3,4], Thomas Henning, PhD[3,5], DiyaaElDin Ashour, PhD[6], Sarah-Lena Puhl, PhD[6], Giuseppe Rizzo, PhD[7], Clément Cochain, PhD[7,8], Tobias Krammer, PhD[9], Alexander Leipold, MSc[9,10], Antoine-Emmanuel Saliba, PhD[9,10], Matthias Mack, MD[11], Nicole Ziegler, PhD[12], Nancy Ernst, PhD[13], Ralf Joachim Ludwig, MD[13], Gustavo Campos Ramos, PhD[6,14], Stefan Frantz, MD[6,14], Lars Dölken, MD[3,5] and Brenda Gerull, MD[1,14,*]

[1]Comprehensive Heart Failure Center, Department of Cardiovascular Genetics, University Hospital Würzburg, Würzburg, Germany.
[2]Comprehensive Heart Failure Center, Department of Nuclear Medicine, University Hospital Würzburg, Würzburg, Germany.
[3]Institute for Virology and Immunobiology, University of Würzburg, Würzburg, Germany.
[4]The Rockefeller University, New York City, USA 10065.
[5]Institute of Virology, Hannover Medical School, Hannover, Germany.
[6]Comprehensive Heart Failure Center, Department for Translational Research, University Hospital Würzburg, Würzburg, Germany.
[7]Institute for Experimental Biomedicine, University Hospital Würzburg, Würzburg, Germany.
[8]Université Paris Cité, PARCC, INSERM, F-75015 Paris, France.
[9]Helmholtz Institute for RNA-based Infection Research (HIRI), Helmholtz-Centre for Infection Research (HZI), Würzburg, Germany.
[10]University of Würzburg, Faculty of Medicine, Institute of Molecular Infection Biology (IMIB), Würzburg, Germany.
[11]University Hospital Regensburg, Department Nephrology, Regensburg, Germany.
[12]Fraunhofer Institute for Translational Medicine and Pharmacology ITMP, Frankfurt am Main, Germany.

[13]Lübecker Institute for Experimental Dermatology LIED, Lübeck, Germany.
[14]Department of Internal Medicine I, University Hospital Würzburg, Würzburg, Germany.

[#]These authors contributed equally.

[*]**Correspondence to:** Brenda Gerull, MD. Email: Gerull_B@ukw.de. Comprehensive Heart Failure Center (CHFC) and Department of Medicine I, University Hospital Würzburg, Am Schwarzenberg 15, 97078 Würzburg, Germany.

Short Title: Murine CMV infection unmasks *Pkp2*-cardiomyopathy

Keywords: Genetic cardiomyopathy, PKP2, TTN, CMV, macrophages, inflammation

List of nonstandard abbreviations: ARVC/ACM – Arrhythmogenic right ventricular cardiomyopathy/Arrhythmogenic cardiomyopathy, PKP2 – plakophilin-2, DCM – Dilated cardiomyopathy, TTN – titin, MCMV – Murine cytomegalovirus, CCL2 – C-C motif chemokine ligand 2, CCR2 – C-C chemokine receptor type 2

Total Word Count: ca. 5600

2. Abstract

Background: Genetic cardiomyopathies display variable penetrance and phenotypic expression, highlighting the influence of environmental modulators. Myocarditis, commonly triggered by cardiotropic viruses, overlaps clinically with genetic cardiomyopathies. Consequently, these infections are implicated as secondary factors that accelerate disease onset and progression, yet their precise impact in specific genetic settings remains unexplored.

Methods: To interrogate this, genetic mouse models heterozygous for a mutant allele of desmosomal plakophilin-2 (*Pkp2*$^{+/-}$) or sarcomeric titin (*Ttn*$^{+/-}$), genes frequently linked to acute myocarditis, were challenged with murine cytomegalovirus (MCMV) to determine how latent infection influences myocardial inflammation, tissue remodeling, and cardiac performance. Integrated experimental approaches, including echocardiography, histology, flow cytometry, single-cell RNA sequencing, as well as cytokine and kinome analyses, defined immune and signaling responses in infected versus non-infected hearts.

Results: Acute, MCMV-induced viral myocarditis and subsequent latent MCMV infection unmasked early disease onset in *Pkp2*$^{+/-}$ animals, leading to progressive systolic impairment, whereas in *Ttn*$^{+/-}$ mice cardiac structure and function remained preserved throughout infection. Cardiac immune profiling uncovered infection- and genotype-specific divergence: both genetic models showed a stable myocardial effector-memory CD8^{+} T-cell response to MCMV, but only *Pkp2*$^{+/-}$ hearts recruited additional Ly6C^{+} CCR2^{+} monocytes and macrophages with distinct inflammatory signatures. In the absence of infection, *Pkp2* insufficiency initiated subclinical CCL2 secretion and subsequent recruitment of CCR2^{+} cells, reflecting early immune

activation preceding age-associated functional and structural decline. At this stage, cytokine and kinase evaluations indicated a balance between proinflammatory and compensatory signals. However, with aging or following MCMV challenge, this balance shifted towards persistent inflammation, evidenced by chronic upregulation of cytokines and activation of signaling pathways, which ultimately led to adverse effects and myocardial dysfunction.

Conclusions: Manifestation of genetic cardiomyopathies depends on interactions between inherited susceptibility and environmental stressors. Here, we show that cytomegalovirus infection intensifies inflammation in *PKP2*-related cardiomyopathy. In contrast, *TTN*-linked cardiomyopathy does not exhibit increased inflammation under the same conditions. For individuals carrying desmosomal variants, infection control and tailored anti-inflammatory strategies may attenuate or delay disease manifestation and progression.

3. Introduction

Clinical presentation and outcomes of patients with cardiomyopathies are determined by a combination of genetic and environmental factors. Among these, viral infections are thought to represent a contributing factor by initiating early cardiac damage and innate immune responses, leading to an acute stage of an inflammatory myopericardial syndrome (IMPS)[1]. Acute myocarditis-like episodes have been reported, especially in patients with arrhythmogenic right ventricular cardiomyopathy/arrhythmogenic cardiomyopathy (ARVC/ACM)[2]. Cardiotropic viruses, such as enterovirus, adenovirus and cytomegalovirus, have been detected in sporadic cases[3], suggesting a pathogenic link between ACM and viral infection. This has led to the hypothesis that pathogenic variants in desmosomal genes could increase the heart muscle's susceptibility to viral infections or inflammation. In this context, genetic alterations in desmoplakin (DSP) are frequently associated with myocarditis-like symptoms[2]; however, genetic variants in the most common disease-associated gene, plakophilin-2 (PKP2)[4], exhibit similar clinical features[5,6]. Heterozygous PKP2 variants show incomplete penetrance, resulting in a broad spectrum of phenotypes, ranging from patients with severe arrhythmias and heart failure to asymptomatic carriers[3]. As a result, the impact of non-genetic factors, especially viral infections, is gaining increasing importance. A recent meta-analysis revealed a high prevalence of pathogenic or likely pathogenic gene variants, notably in the sarcomeric gene titin (TTN) in addition to desmosomal genes (DSP, PKP2, and DSG2) among adults with myocarditis[7]. The presence of these gene variants coupled with acute myocarditis has been linked to a higher risk of adverse cardiovascular events, highlighting an essential connection between inflammation and accelerated disease progression in cardiomyopathies[8].

62 Titin truncating variants (TTNtv) are a common cause of dilated cardiomyopathy
63 (DCM), accounting for up to 25% of cases[9]. Several modifying factors, including
64 pregnancy, alcohol abuse, chemotherapy, and other comorbidities, contribute to overt
65 disease[10]. Besides numerous human studies, we previously demonstrated that second
66 hits like angiotensin II or isoproterenol led to the development of cardiomyopathy with
67 cardiac dysfunction and fibrotic remodeling in a mouse model carrying an A-band Ttn
68 truncating variant[11], however, the role of viral infections remains unknown, even though
69 cardiotropic viruses have been detected in endomyocardial biopsies of DCM patients[12].
70 Animal models are therefore essential to dissect how secondary triggers interact with
71 genetic susceptibility, shape immune activation and determine the timing of therapeutic
72 interventions. Therefore, we aimed to study the mechanistic interplay among genetic
73 predispositions, viral pathogenesis, and immune responses during infection with the
74 common viral pathogen cytomegalovirus (CMV) in murine models of cardiomyopathy.

75 Human CMV infections generally remain subclinical in healthy individuals, but have
76 been associated with cardiovascular diseases such as myocarditis. Additionally,
77 seropositivity and lifelong latency are linked to a higher risk of developing inflammatory
78 diseases later in life[13,14]. CMV can infect various cells in peripheral organs, including
79 the heart, triggering typical immune responses involving innate and adaptive immune
80 cells. Murine CMV (MCMV) closely resembles human CMV, mimicking its primary
81 functional pathways, and is therefore used to study the acute and latent effects of viral
82 infections on cardiovascular diseases[15].

83 Consequently, we examined the effects of MCMV infection as a second hit in two
84 heterozygous genetic mouse models that mimic *PKP2*- and *TTN*-associated genetic
85 predispositions. Interestingly, we observed distinct outcomes regarding the
86 development of cardiomyopathy and the role of the innate immune system in the

87 disease process. Heterozygous cardiac-restricted *Pkp2*$^{+/-}$ mice developed progressive
88 cardiac dysfunction linked to a myeloid cell and cytokine-driven inflammatory
89 response. In contrast, hearts of *Ttn*$^{+/-}$ mice remained unaffected despite an appropriate
90 MCMV-associated T-cell response. Furthermore, detailed age- and time-dependent
91 analyses of cardiac immune cell composition, cytokines, and their receptors in *Pkp2*$^{+/-}$
92 mice indicate an early, intrinsic role for the CCL2-CCR2 axis and suggest a potential
93 therapeutic window for targeted inflammatory therapies.

4. Methods

All mouse studies and animal numbers used were in compliance with the Directive 2010/63/EU of the European Parliament, approved by the local ethics committee (RUF-55.2.2-2532-2-663, RUF-55.2.2-2532-2-962, and RUF-55.2.2-2532-2-1244) and conducted in accordance with the institutional guidelines.

Data Availability

A detailed methods section and all data supporting the findings of this study are provided within the article and its Supplemental Material. The RNA sequencing dataset is available from the NCBI Gene Expression Omnibus (GEO) under the GSE311777 accession number.

5. Results

Cardiomyocyte-specific heterozygous loss of *Pkp2* reveals normal myocardial structure, function and immune cell composition

To investigate how loss of one or both alleles of PKP2 affects cardiac structure, function, myocardial inflammation and immune responses in a cardiac-specific manner, we intercrossed *Pkp2* floxed mice with Cre-deleter mice in which the Cre recombinase gene is expressed under the control of the α-myosin heavy chain (αMHC) promoter which yielded homozygous (*Pkp2*$^{-/-}$, Figure 1A; S1A) and heterozygous (*Pkp2*$^{+/-}$) knock-out mice. Homozygous loss of PKP2 protein (Figure S1B+C) did not induce premature mortality, but caused marked biventricular dysfunction at 6-8 weeks of age compared to age-matched control (Ctr) animals (Figure 1B; Table S1). Consistent with this, picrosirius red (PSR) staining revealed significantly increased collagen deposition in both ventricles (Figure 1C). However, flow cytometry showed no differences in total CD45^{+} leukocytes, monocytes/macrophages or infiltrating Ly6C^{+} monocytes compared to Ctr, suggesting no active cell-based immune response at this already advanced stage of disease (Figure 1D).

Since ACM is inherited in an autosomal dominant manner[16], we analyzed *Pkp2*$^{+/-}$ mice, which more closely reflect the human condition (Figure 1E). Consistent with findings from other monoallelic desmosomal models[17-19], *Pkp2*$^{+/-}$ mice showed structurally and functionally normal hearts at 9 months of age: left ventricular end-diastolic diameter (LVEDD), left ventricular ejection fraction (LVEF) and tricuspid annular plane systolic excursion (TAPSE) were preserved, while myocardial collagen content or immune cell infiltration were not increased (Figure 1F-H; Table S2).

128 **MCMV infection causes progressive cardiac dysfunction in *Pkp2*$^{+/-}$ hearts**

129 The absence of an overt phenotype in *Pkp2*$^{+/-}$ mice provides an opportunity to examine
130 how viral triggers interact with genetic predisposition and cardiac immune responses
131 to potentially trigger disease. To assess this, 3-month-old *Pkp2*$^{+/-}$ and Ctr mice were
132 infected with 5x10^{5} plaque forming units (PFU) Δm157-MCMV-eGFP (MCMV), a
133 mutant strain that bypasses natural killer (NK) cell-mediated clearance in C57BL/6J
134 mice and ensures productive infection[20]. Mice of both genotypes received phosphate-
135 buffered saline (PBS) as a control (Figure 2A). Analyses covered time points of acute
136 (5-14 days post-infection, dpi), sub-acute (1 month post-infection, mpi) and latent
137 MCMV infection (3; 6mpi). Both infected genotypes developed splenomegaly during
138 acute infection, indicating immune system activation (Figure 2B). Hematoxylin-eosin
139 (HE) and immunostaining revealed myocardial immune infiltrates composed primarily
140 of CD8^{+} T-cell plaques and scattered CD4^{+} T-cells in either genotype during the acute
141 phase (Figure 2C; Figure S2A). Quantitative PCR for the viral *ie1* gene confirmed viral
142 DNA persistence in heart, salivary gland and lung with a gradual decline from acute to
143 latent stages (Figure 2D; Figure S2B+C). Serial echocardiography from 1 to 6mpi
144 demonstrated a progressive decline in LVEF exclusively in MCMV-infected *Pkp2*$^{+/-}$
145 mice as of 3mpi and worsening by 6mpi, while LVEDD remained stable across all
146 groups (Figure 2E; Table S3-S6). Collagen content increased with age in all groups in
147 a genotype- and infection-independent manner (Figure 2F+G, Figure S2D-F). CD8^{+} T-
148 cell numbers decreased from 1 to 6mpi in both infected genotypes, but remained higher
149 than in non-infected hearts (Figure 2H; Figure S2G; Table S7). Flow cytometry at 6mpi
150 identified CD8^{+} KLRG1^{+} terminally differentiated effector memory T-cells as the
151 dominant expanded population, consistent with MCMV-induced memory inflation in the
152 CD8^{+} T-cell compartment[21]. Strikingly, monocytes/macrophages appeared more

153 abundant in *Pkp2*$^{+/-}$ MCMV than in Ctr MCMV hearts (Figure 2I, Figure S3). Together,
154 these findings show that while MCMV infection induces T-cell infiltration and persistent
155 viral DNA in both genotypes, *Pkp2*$^{+/-}$ MCMV mice selectively develop progressive
156 systolic dysfunction accompanied by monocyte/macrophage accumulation,
157 establishing MCMV as a potent trigger of cardiac disease onset in *Pkp2*$^{+/-}$ mice.

158 **CITE-seq and transcriptomic profiling reveal genotype-dependent and virus-**
159 **specific alterations of the cardiac immune compartment**

160 To define immune cell composition in chronically infected hearts, we performed cellular
161 indexing of transcriptomes and epitopes by sequencing (CITE-seq) of ventricular
162 CD45^{+} leukocytes at 6mpi, excluding circulating cells by intravenous anti-CD45.2-APC
163 injection. Two independent experiments were performed, each including 10 pooled
164 samples (non-infected groups, n=2; MCMV groups, n=3), labeled with TotalSeq-A
165 hashtags that were used for demultiplexing (Figure 3A; Figure S4A; Supplemental
166 Methods). After quality control, doublet removal, and dataset integration (Figure S4B),
167 26,656 cells remained for further analysis. Initial clustering defined 16 immune cell
168 groups that were annotated using canonical lineage markers for T-cells (CD3, TCRβ),
169 B cells (CD19), NK cells (NK1.1), neutrophils (Ly6G), dendritic cells (CD11c),
170 monocytes (Ly6C), and macrophages (CD64, CD88). Sub-clustering of the lymphoid
171 and myeloid compartments refined the annotation to 23 distinct populations, defined
172 by combined transcriptomic and protein signatures (Figure S5).

173 Dimensional reduction and compositional analyses revealed infection- and genotype-
174 dependent reshaping of the cardiac immune landscape. In both genotypes, latent
175 MCMV infection induced robust expansion of effector T-cell subsets, including
176 activated CD4^{+} Th1 cells (CD4_Th1_act; *Cd4, Cd28, Ctla4*), tissue-resident memory-

177 like CD8$^+$ effectors (CD8_TRM_like; *Cd8a, Itga1, Gzmk, Klrc1*), terminal KLRG1$^+$
178 effector memory (CD8_Teff_KLRG1+; *CD8a, Klrg1, Gzmb, Ccl5*), and proliferating
179 CD8$^+$ T cells (CD8_Teff_prolif; *Mki67, Top2a, Birc5*). Beyond this shared antiviral
180 response, *Pkp2*$^{+/-}$ MCMV hearts displayed a distinct myeloid signature with a marked
181 increase in cDC1 (*Xcr1, Clec9a, Itgae*) and antigen-presenting cDC2 cells (*Cd209a,*
182 *Bhlhe40, Dpp4*), as well as in two subsets of monocyte-derived macrophages. These
183 comprised a pro-inflammatory subset (moMac_Ly6C$^+$_inflam; *Plac8, Chil3, Ly6c2*) and
184 a reparative *Trem2*$^+$*Spp1*$^+$ subset (moMac_Trem2$^+$_Spp1$^+$; *Trem2, Spp1, Fabp5*), the
185 latter previously associated with profibrotic and tissue-remodeling functions in the
186 infarcted heart[22]. Interestingly, these subsets were already elevated in non-infected
187 *Pkp2*$^{+/-}$ myocardium compared to Ctr non-infected hearts, indicating genotype-
188 dependent priming of the myeloid compartment in the *Pkp2* heterozygous setting
189 (Figure 3B+C). No additional populations were selectively enriched in the *Pkp2*$^{+/-}$
190 MCMV group, indicating convergence of viral and genetic factors on a common
191 immune response. To validate these compositional shifts, we performed differential
192 abundance testing using the MiloR framework, comparing *Pkp2*$^{+/-}$ non-infected and
193 *Pkp2*$^{+/-}$ MCMV hearts to Ctr non-infected mice, thereby allowing assessment of
194 genotype-dependent baseline changes and infection-driven responses on the *Pkp2*$^{+/-}$
195 background. moMac_Ly6C+_inflam, cDC1, and cDC2 populations were significantly
196 enriched when comparing non-infected *Pkp2*$^{+/-}$ and Ctr hearts, confirming genotype-
197 dependent expansion of myeloid subsets. Following MCMV infection (*Pkp2*$^{+/-}$ MCMV
198 vs. Ctr non-infected), CD8_TRM_like and CD8_Teff_KLRG1+ populations overall
199 displayed the strongest expansion, while the underlying *Pkp2*-dependent myeloid
200 alterations persisted (Figure 3D; Figure S6A).

201 To identify inflammatory mediators underlying these compositional changes, we
202 performed differential expression analysis of cytokines and their receptors across all
203 immune cell types (Figure 3E). Even in the absence of infection, non-infected *Pkp2*$^{+/-}$
204 hearts showed a distinct pro-inflammatory profile: *Ccr2* was strongly upregulated,
205 indicating enhanced recruitment and activation of monocytes and macrophages via
206 ligands like *Ccl2, Ccl7 or Ccl12*[23]. Elevated expression of *Il1b*, *Il1a,* and *Il6* further
207 supported activation of innate inflammatory pathways, while increased *Il17r* and *Il17ra*
208 indicated responsiveness to IL-17 signaling, typically associated with pro-inflammatory
209 Th17 cells[24]. In both genotypes, MCMV induced upregulation of *Ccl5*, *Ifng* and its
210 receptor *Ifngr1*, as well as *Il2rg* and *Il2rb*, components of the interleukin-2 receptor,
211 implicated in regulating infection-associated T-cell responses[25,26]. In addition, inhibitory
212 molecules such as *Ctla4* were upregulated (Figure 3E). When comparing *Pkp2*$^{+/-}$
213 MCMV to Ctr MCMV to isolate the genotype effect, a persistent myeloid-dominant
214 inflammatory signature emerged – again driven by *Ccr2* and related mediators already
215 identified in the *Pkp2*$^{+/-}$ non-infected hearts (Figure S6B).

216 Finally, pseudobulk differential expression was performed per cell type and subjected
217 to pathway enrichment analysis using the database MSigDB Hallmarks. In
218 Mac_TRM_MHCII+ macrophages, both comparisons (*Pkp2*$^{+/-}$ non-infected vs. Ctr non-
219 infected; *Pkp2*$^{+/-}$ MCMV vs. Ctr non-infected) revealed consistent enrichment of
220 immune activation pathways, with TNF-α signaling via NF-κB as the top hit. Additional
221 pathways included IL-6/JAK/STAT3 signaling, IL-2/STAT5 signaling and a broad
222 inflammatory response signature (Figure 3F, Figure S6C). Consistently, STAT3 protein
223 levels were increased in infected and non-infected *Pkp2*$^{+/-}$ mice (Figure S6D).
224 Together, single-cell RNA and CITE-sequencing captured a subclinical accumulation
225 and activation of specific monocyte/macrophage populations already in phenotypically

226 unaffected non-infected *Pkp2*$^{+/-}$ mice, similar to those observed in *Pkp2*$^{+/-}$ MCMV mice
227 with systolic dysfunction. Therefore, the mutation itself already reshapes the cardiac
228 immune landscape. Nevertheless, an additional trigger is required to actually cross the
229 threshold for developing a clinical phenotype.

230 **The important role of the CCL2-CCR2 axis**

231 Next, we sought to identify soluble mediators that might attract or maintain
232 inflammatory cells in whole-heart protein samples and serum. This was done using
233 proximity extension assay-based proteomics at 6mpi (corresponding to 9 months of
234 age). Given the strong *Ccr2* upregulation observed in cardiac leukocytes, we expected
235 to identify one of its attractants *Ccl2, Ccl7* or *Ccl12*[23]. Interestingly, aside from CCL2,
236 several additional mediators were significantly upregulated in phenotypically
237 unaffected *Pkp2*$^{+/-}$ hearts (Figure 1E-H), including chemokines involved in monocyte
238 and macrophage recruitment (CCL2, CCL4, CXCL1), pro-inflammatory cytokines (IL-
239 1β) and immunoregulatory mediators (PD-L2, CCL22). Additionally, the metabolic
240 regulator FGF21 was increased and has been reported to exert cardioprotective
241 effects[27,28]. In contrast, these factors were not elevated in serum. This cytokine
242 response was amplified upon MCMV infection in *Pkp2*$^{+/-}$ mice: in addition to FGF21,
243 CCL2, CXCL1, CCL22, and CCL4, we observed upregulation of CCL12 and CCL5. In
244 serum, the most prominent change was a slight induction of IL-6, consistent with
245 systemic MCMV-driven inflammation, whereas heart-specific mediators remained
246 largely unchanged, indicating a predominantly local cardiac response (Figure 4A;
247 Figure S7A-C; Table S8+S9). Thus, these findings demonstrate that *Pkp2*-deficiency
248 alone is sufficient to elicit an early subclinical pro-inflammatory milieu in the heart,
249 consistent with recruitment of pro-inflammatory Ly6C^{+} CCR2^{+} monocytes. Even though

MCMV induced a CD8$^+$ T-cell response, this was associated with only a modest change in the overall cytokine spectrum compared with the genotype-driven signals.

We next examined whether the expansion of myeloid populations in *Pkp2*$^{+/-}$ hearts could be recapitulated using a macrophage-tailored flow cytometry panel. While in *Pkp2*$^{+/-}$ MCMV hearts, Ly6C$^+$ monocytes (typically also CCR2$^+$) and pro-inflammatory macrophages (TIM4$^-$, MHC-II$^+$) were significantly increased, non-infected *Pkp2*$^{+/-}$ hearts, only showed a trend towards an increased abundance of these subsets (Figure 4B+C), indicating that single-cell analysis is more sensitive at detecting an early and cell-specific immune response. Together, these data show that *Pkp2*$^{+/-}$ hearts mount a local cytokine response amplified by MCMV, with recruitment of Ly6C$^+$ CCR2$^+$ monocytes highlighting the CCL2/CCR2 axis as a central driver of myocardial inflammation.

MCMV infection in *Ttn*$^{+/-}$ mice does not induce cardiac dysfunction

To test whether the combined effects of genetic predisposition and viral infection reflect a broader principle in genetic cardiomyopathies, as observed in human myocarditis patients[7], we applied the same experimental setup in mice with a heterozygous global titin truncating mutation (*Ttn*$^{+/-}$), a model developing cardiomyopathy under experimental stress conditions[11,29]. 9-month-old *Ttn*$^{+/-}$ mice were indistinguishable from controls (Ctr), regarding cardiac function, collagen deposition and immune cell abundance (Figure S8A–D). In accordance with the *Pkp2* work, we infected 3-month-old *Ttn*$^{+/-}$ and Ctr mice with 5×10^5 PFU MCMV and performed analyses at 1, 3 and 6mpi (Figure 5A). Non-infected *Ttn*$^{+/-}$ and Ctr mice received PBS and were combined into one control group. Echocardiography and histology showed no genotype- or infection-dependent functional or structural alterations at any time point following

274 infection (Figure 5B+C; Figure S8E+F; Table S10-S13). At 6mpi, immunostaining
275 revealed scattered CD8$^+$ T-cells in infected hearts irrespective of genotype (Figure 5D).
276 Flow cytometry confirmed infection-induced expansion of cytotoxic CD8$^+$ T-cells and
277 KLRG1$^+$ CD8$^+$ T-cells in both genotypes, with no change in monocyte/macrophage
278 numbers (Figure 5E, Figure S8G).

279 To capture subtle immune shifts, CITE-seq was performed on CD45$^+$ cells at 6mpi (10
280 hashed samples: Ctr non-inf n=2, *Ttn*$^{+/-}$ non-inf n=2, Ctr MCMV n=3, *Ttn*$^{+/-}$ MCMV n=3;
281 Figure S9A-C). Relative cell type abundance did not differ between non-infected *Ttn*$^{+/-}$
282 and Ctr hearts, while both infected groups displayed expansion of activated T-cell
283 subsets (CD4_Th1_act, CD8_TRM_like, CD8_Teff_KLRG1+, CD8_Teff_prolif,
284 CD8_Tex_like; Figure 5F+G). Myeloid proportions remained unchanged across all
285 groups, in contrast to the genotype-driven myeloid skewing observed in *Pkp2*$^{+/-}$ mice.
286 MiloR[30] testing confirmed no differences between non-infected genotypes, justifying
287 their pooling in subsequent analyses. MCMV infection (*Ttn*$^{+/-}$ MCMV vs. Ctr non-
288 infected) enriched CD8_TRM_like, NK_eff, CD8_Teff_KLRG1+ and CD8_Tex_like
289 clusters, mirroring findings in Ctr MCMV hearts, while there was no difference between
290 both infected genotypes (Figure 5H; Figure S9D+E). Differential cytokine expression
291 analysis supported these results: *Ttn*$^{+/-}$ non-infected hearts showed no upregulated
292 inflammatory mediators, while MCMV infection induced *Ifng, Ccl5* and IL-2 and IL-12
293 receptor components (*Il2rb, Il12rb2*) in both genotypes compared to non-infected
294 animals (Figure 5I, Figure S9F). Thus, in contrast to *Pkp2*$^{+/-}$ mice, *Ttn*$^{+/-}$ hearts
295 exhibited no genotype-driven immune remodeling. All observed changes were
296 attributable to MCMV infection, underscoring the specificity of immune activation in the
297 *Pkp2*$^{+/-}$ model.

298

299 **Immune cell remodeling and phenotype development in aged *Pkp2*$^{+/-}$ mice**

300 To determine how inflammation, immune responses and cardiac function evolve with
301 age in the absence of viral infection, we longitudinally analyzed *Pkp2*$^{+/-}$ and Ctr mice
302 from 3 to 15 months of age (Figure 6A). Aging progressively reshapes the cardiac
303 immune landscape[31,32]. We thus hypothesized that interaction with *Pkp2* deficiency
304 might eventually unmask a cardiac phenotype.

305 Up to 9 months, *Pkp2*$^{+/-}$ mice maintained normal cardiac function despite a myeloid-
306 skewed inflammatory state (Figures 2E+3D+4A; *Pkp2*$^{+/-}$ non-infected at 6mpi). From
307 12 months onward, however, LVEF declined and LVEDD increased, progressing
308 further by 15 months, while Ctr hearts remained stable, indicating worsening systolic
309 function and ventricular remodeling (Figure 6B; Table S14+S15). Collagen content
310 increased with age in both genotypes but rose more steeply in *Pkp2*$^{+/-}$ hearts, with
311 fibrosis localized to the LV and RV endocardial layers (Figure 6C+D; Figure S10A).
312 Flow cytometry revealed progressive accumulation of inflammatory Ly6C^{+} monocytes
313 and persistently elevated total macrophages in *Pkp2*$^{+/-}$ hearts from 12 months onward.
314 Among macrophage subsets, pro-inflammatory antigen-presenting (TIM4^{-} MHC-II^{+})
315 cells were consistently increased, despite an overall age-related decline in this
316 population (Figure 6E). Cytokine profiling supported these findings: IL-1β, CCL2 and
317 CCL22 were elevated solely in *Pkp2*$^{+/-}$ hearts as of 9 months, while CCL12 increased
318 only at 15 months, whereas none of these mediators were altered in serum, indicating
319 a localized rather than a systemic inflammatory response. Cardioprotective FGF21
320 was already elevated in *Pkp2*$^{+/-}$ hearts as of 9 months and additionally increased in
321 serum at 15 months, suggesting an emerging compensatory systemic response. In
322 contrast, IL-10 remained unchanged in cardiac tissue but was reduced in serum,
323 consistent with a shift towards a pro-inflammatory milieu in *Pkp2*$^{+/-}$ mice (Figure 6F;

324 Table S16+17). Together, these data show that physiological aging unmasks systolic
325 dysfunction, LV dilation, fibrosis and a sustained cardiac inflammatory state in *Pkp2*$^{+/-}$
326 mice. Between 9 and 12 months, inflammatory markers rise before the onset of overt
327 fibrosis and contractile decline, defining a therapeutic window during which anti-
328 inflammatory intervention may attenuate immune activation and fibrotic remodeling to
329 preserve cardiac function.

330 To identify signaling networks associated with this early inflammatory state, kinome
331 profiling was performed in 12-month-old *Pkp2*$^{+/-}$ versus Ctr hearts. The significantly
332 regulated kinases were uniformly upregulated, indicating a coordinated activation of
333 inflammatory, immune, and compensatory signaling pathways (Figure 7A; Figure
334 S10B). IKBKE, PRKD1 and CSNK2A1 reflect activation and regulation of the NF-κB
335 pathway[33,34] sustaining chronic low-grade inflammation. FES, FGR, LCK and EPHA1
336 indicate enhanced immune-cell signaling and cell-cell communication, supporting the
337 immune activation observed at this stage. In parallel, MET, AKT3, PRKG1/2, CSNK2A1
338 and RPS6KB2 suggest engagement of pro-survival and metabolic stress-response
339 pathways via PI3K-AKT-mTOR signaling[35]. STRING network analysis showed
340 connections between these immune-related and compensatory kinases (Figure 7B),
341 while KEGG pathway enrichment also reflected the dual activation of different pro-
342 inflammatory signaling pathways alongside pro-survival cascades, indicating cardiac
343 stress adaptation (Figure 7C). To assess whether kinase activation translated into
344 downstream pathway engagement at later stages, we analyzed hearts from 15-month-
345 old mice by Western blot (Figure 7D). Consistent with persistent NF-κB activation, both
346 total and phosphorylated p65 (p_i-p65) were increased in *Pkp2*$^{+/-}$ hearts compared with
347 Ctr. These molecular changes coincide with the stage of functional decline and fibrosis

348 in aged *Pkp2*$^{+/-}$ hearts, confirming sustained NF-κB signaling and chronic inflammatory
349 stress.

350 **Early inflammatory signatures in homozygous *Pkp2*$^{-/-}$ hearts point towards**
351 **infiltrating monocytes as a therapeutic target**

352 The overall phenotype of heterozygous *Pkp2*$^{+/-}$ mice was moderate and became
353 apparent only upon the inflammatory trigger and at advanced age. To model a more
354 pronounced phenotype, we analyzed homozygous *Pkp2*$^{-/-}$ mice. Because 6-8-week-
355 old *Pkp2*$^{-/-}$ hearts already displayed extensive fibrosis (Figure 1C), mice were
356 examined at 3-4 weeks to capture earlier inflammatory stages (Figure 8A). However,
357 even at this age, echocardiography revealed functional impairment, albeit less
358 pronounced than at 6-8 weeks (Figure 8B). Interestingly, HE-stained hearts showed
359 clear immune cell accumulation between cardiomyocytes in both ventricles, which
360 stained positive for the macrophage marker CD68 (Figure 8C+D). Flow cytometry
361 confirmed significant infiltration of F4/80^{+} macrophages and Ly6C^{+} monocytes in *Pkp2*$^{-}$
362 $^{/-}$ hearts. Sub-characterization revealed expansion of recruited pro-inflammatory (TIM4^{-}
363 MHC-II^{+}) and tissue-injury-associated macrophages (TIM4^{-} MHC-II^{-}), alongside
364 reduced tissue-resident macrophages (TIM4^{+} MHC-II^{-}), indicating a monocyte-derived
365 inflammatory response and identifying these cells as a potential therapeutic target
366 (Figure 8E). Cytokine analysis showed broad induction of inflammatory mediators in
367 *Pkp2*$^{-/-}$ hearts, including monocyte/macrophage chemoattractants (CCL2, CCL12,
368 CCL4, CCL22, CCL5), neutrophil chemokines (CXCL1, CXCL2), eosinophil-recruiting
369 CCL11 and pro-inflammatory cytokines (IL-1α, IL-1β). Upregulation of immune
370 checkpoints PD-L2 and CTLA4 suggested active immunoregulation within the
371 myocardium. These changes were largely heart-restricted, with serum mediators

372 mainly unaltered (Figure 8F). Recruitment of CCR2^{+} monocytes via CCL2 and CCL12
373 thus represents a central feature of the *Pkp2*$^{-/-}$ model.

374 To examine whether this monocyte-driven inflammatory state can be modulated, we
375 treated 3-week-old *Pkp2*$^{-/-}$ and Ctr mice with an anti-CCR2 antibody (Figure 8G).
376 Treatment duration was limited to 7 days to prevent the formation of anti-drug
377 antibodies, which could compromise target engagement[36]. At the beginning of
378 treatment, mild fibrotic remodeling was already evident in *Pkp2*$^{-/-}$ hearts (Figure 8H).
379 Despite this, CCR2 blockade markedly reduced total cardiac
380 monocytes/macrophages, with similar trends toward decreases in Ly6C^{+} monocytes,
381 F4/80^{+} macrophages (Figure 8I), tissue-injury-associated and pro-inflammatory
382 subsets (Figure S11A+B), confirming the monocytic origin of the likely disease-driving
383 myeloid populations in this model. Fibrosis and cardiac function remained unchanged
384 due to the short treatment period (data not shown). These data confirm effective
385 depletion of CCR2^{+} myeloid populations *in vivo* and indicate that the cellular and tissue
386 state at treatment onset likely shapes the measurable downstream effects.

387 Across genetic, viral and aging models, our data show that, in particular, the *Pkp2*$^{+/-}$
388 genotype and therefore disturbed desmosomal proteins predispose to immune
389 remodeling that accelerates with secondary stressors, whereas complete loss of *Pkp2*
390 rapidly triggers monocyte-driven inflammation and cardiac dysfunction, highlighting
391 inflammatory monocytes as a therapeutic target population.

392 **6. Discussion**

393 In this study, we demonstrate that murine cytomegalovirus (MCMV) infection acts as a
394 potent, genotype-dependent environmental modifier, unmasking early disease in
395 phenotypically unaffected cardiac-restricted *Pkp2*$^{+/-}$ mice, but not in *Ttn*$^{+/-}$ mice. While
396 both models exhibited persistent effector-memory CD8^{+} T-cells in the myocardium
397 during latent infection, only *Pkp2*$^{+/-}$ MCMV mice developed progressive systolic
398 dysfunction accompanied by increased recruitment of monocytes and macrophages -
399 findings that were absent in *Ttn*$^{+/-}$ MCMV mice. These results reveal that MCMV does
400 not trigger a generic response in genetic cardiomyopathies, but instead amplifies
401 desmosome-related inflammation, driving ACM-like pathology. Even in the absence of
402 infection, the *Pkp2*$^{+/-}$ genotype alone induced a subclinical pro-inflammatory state,
403 which is mediated by the CCL2/CCR2 signaling pathway. With aging, *Pkp2*$^{+/-}$ mice
404 developed fibrosis and overt contractile dysfunction in the absence of MCMV, marking
405 a transition from compensated inflammation to pathological remodeling. Together,
406 these findings establish viral infection as a disease-modifying factor in ACM, delineate
407 mutation-specific inflammatory mechanisms distinguishing ACM from other
408 cardiomyopathies, and identify the subclinical inflammatory phase as a promising
409 therapeutic window for anti-inflammatory intervention.

410 As a cardiotropic virus with high seroprevalence in the human population, CMV
411 establishes lifelong latency and can reactivate, for instance, under inflammatory
412 stress[37,38]. MCMV closely mirrors the human infection, reproducing key virological and
413 immunological features, including reshaping of the T-cell compartment through
414 memory inflation, which maintains chronic low-grade inflammation[21]. To prevent rapid
415 NK cell-mediated clearance typical for wild-type MCMV in C57BL/6 mice, we used a

416 m157-deficient strain (Δm157-MCMV-eGFP) that bypasses recognition by the
417 activating NK cell receptor Ly49H and shifts the antiviral defense toward a sustained
418 $CD8^+$ T-cell response[20,39]. Consistently, we observed prominent $CD8^+$ T-cell plaques in
419 acutely infected hearts that declined but persisted up to 6mpi. A subset of these cells
420 expressed KLRG1, indicating an effector-memory phenotype characteristic of CMV-
421 driven memory inflation and a chronic pro-inflammatory milieu[40]. Importantly, Ctr
422 MCMV mice in both genetic models did not develop systolic dysfunction or fibrosis,
423 reflecting asymptomatic latent infection in immunocompetent hosts. In contrast, *Pkp2*$^{+/-}$
424 mice with latent MCMV infection developed progressive systolic dysfunction without
425 structural remodeling, establishing MCMV as a potent second hit that unmasks disease
426 in a genetically primed background. Infection amplified the pre-existing inflammatory
427 state in *Pkp2*$^{+/-}$ mice, marked by early cytokine activation and myeloid cell recruitment.
428 At the same time, additional $CD8^+$ T-cell infiltration further enhanced cytokine signaling
429 and was associated with functional decline. Previous studies have shown that chronic
430 inflammatory mediators can exert negative inotropic effects[41] and destabilize
431 desmosomal integrity[42], thereby impairing cardiac contractility, providing a possible
432 explanation for the observed phenotype in our model. However, this MCMV-induced
433 phenotype was genotype-specific. *Ttn*$^{+/-}$ mice carrying a truncating titin variant[11],
434 despite mounting a similar $CD8^+$ T-cell response, showed preserved cardiac function
435 and no signs of additional inflammation throughout the entire time course. Previous
436 studies demonstrated that stimulation with angiotensin II or isoproterenol induced
437 systolic failure and fibrosis in phenotypically silent *Ttn*$^{+/-}$ mice, indicating that the
438 described pathology is linked to biomechanical rather than inflammatory stress[11,29].
439 Thus, the mechanisms by which *Pkp2* and *Ttn* mutations lead to cardiomyopathy
440 diverge: desmosomal disruption generates an intrinsic pro-inflammatory state that viral

infection can amplify, whereas titin mutation-driven disease appears to be dominated by stress-responsive or possibly autoimmune mechanisms. Together, these findings establish CMV as a context-dependent modifier of genetic cardiomyopathy in mice, revealing that viral infection amplifies mutation-specific immune mechanisms rather than acting as a universal pathogenic trigger across genotypes and model systems.

In the absence of external triggers, *Pkp2*$^{+/-}$ mice exhibited a slowly progressive phenotype that mirrors the clinical trajectory of ACM, transitioning from a concealed phase to overt cardiac dysfunction. Cardiac function remained preserved up to 9 months of age, followed by the onset of interstitial fibrosis and contractile impairment from 12 months onward. Molecularly, this progression was preceded by early upregulation of CCL2, a chemoattractant for cells expressing its receptor CCR2, along with increased IL-1β signaling in *Pkp2*$^{+/-}$ hearts. These changes promoted the recruitment of Ly6C^{+} CCR2^{+} monocytes and, ultimately, pro-inflammatory macrophages. These events parallel findings in *Dsg2*-based ACM models, where *Ccl2/Ccr2* upregulation and macrophage influx were identified as an early sign of the disease process[18,43]. In addition, we identified *Trem2*$^{+}$*Spp1*$^{+}$ macrophages resembling the reparative *Trem2*^{hi}*Spp1*^{hi} population described after myocardial infarction (MI)[44]. Unlike the sequential inflammatory-to-reparative transition seen after MI, Ly6C^{+} CCR2^{+} monocytes and *Trem2*$^{+}$*Spp1*$^{+}$ macrophages coexisted in *Pkp2*$^{+/-}$ hearts, indicating persistent low-grade signaling that sustains both inflammatory and pro-fibrotic programs. In a model of acute viral myocarditis, *Spp1*$^{+}$ macrophages instead adopted a pro-inflammatory role by inducing fibroblast *Ccl2/Ccl7* expression and promoting CCR2^{+} cell recruitment[45]. These findings highlight the environment-dependent heterogeneity of macrophage function in acute and chronic settings. At 9 months, apart from pro-inflammatory molecules, several immunoregulatory mediators were elevated,

466 including CCL22, which attracts regulatory T cells[46]; PD-L2, a ligand of the PD-1
467 checkpoint receptor that dampens T-cell activation[47]; and FGF21, a cytokine with
468 cardioprotective effects in mice limiting cardiac damage in hypertension and oxidative
469 stress[27,28]. These changes suggest an early balance between pro- and anti-
470 inflammatory signals. With age, this equilibrium shifted toward chronic inflammation,
471 reflected by CCL12 expression at 15 months and also in *Pkp2*$^{+/-}$ MCMV hearts at 6mpi.
472 A similar *Ccl12* induction has been reported in *Dsg2*^{cKO} mice during late stages of
473 disease, consistent with a shared inflammatory program driving CCR2^{+} cell
474 recruitment[43]. Moreover, in the setting of MI combined with chronic periodontal
475 inflammation, *Ccl12* was shown to prolong inflammation and impair cardiac wound
476 healing, underscoring its role in sustaining maladaptive immune responses[48]. Kinome
477 profiling at 12 months revealed concurrent activation of immune-cell kinase networks
478 and stress-response pathways. Upregulated kinases included IKBKE and PRKD1,
479 both activators of NF-κB[33,34], and FGR, FES and LCK, linked to myeloid and lymphoid
480 signaling[49-51], together indicating sustained innate immune activation.
481 Correspondingly, phosphorylated p65 and total p65 were elevated in 15-month-old
482 *Pkp2*$^{+/-}$ hearts, confirming persistent NF-κB activity. While NF-κB-mediated monocyte
483 recruitment has been described in *Dsg2*$^{mut/mut}$ models[52], our data extend this
484 mechanism to heterozygous *Pkp2* deficiency. Interestingly, Pérez-Hernández et al.
485 also identified NF-κB as a transcription factor associated with PKP2, implying that
486 PKP2 deficiency makes cardiomyocytes more prone to sterile myocarditis, which can
487 be worsened by inflammatory or viral triggers[53], as shown in our study. Integrating
488 these findings, we propose that the *Pkp2*$^{+/-}$ genotype intrinsically activates NF-κB-
489 dependent signaling in cardiomyocytes, driving sustained release of CCL2 and, at later
490 stages, CCL12. This chemokine profile promotes recruitment of CCR2^{+} monocytes and

impairs resolution of inflammation, resulting in the persistence of macrophages with both inflammatory and pro-fibrotic properties. Such inflammatory activation was absent in *Ttn*$^{+/-}$ hearts, underscoring the genotype-specific nature of this response. In *Pkp2*$^{+/-}$ hearts, sustained macrophage activity likely drives progressive injury by releasing proteases and reactive oxygen species[54], which promote extracellular matrix remodeling and systolic dysfunction. Identifying this inflammatory phase before irreversible fibrosis develops defines a promising window for therapeutic intervention.

Building on this CCR2-centered mechanism, studies in *Dsg2*$^{mut/mut}$-based ACM have demonstrated that genetically blocking CCR2-dependent monocyte recruitment reduces macrophage-driven fibrosis[52], supporting the idea that CCR2^{+} cells directly contribute to desmosomal injury. In our *Pkp2*$^{-/-}$ model, CCR2^{+} macrophages were similarly the predominant expanded population, and short-term anti-CCR2 treatment showed effective depletion *in vivo*. Even though the intervention was initiated when fibrotic changes were already present, the reduction in CCR2^{+} myeloid cells suggests that blocking this pathway at an earlier, inflammation-dominated stage would probably exert a more pronounced effect - consistent with findings from the *Dsg2*$^{mut/mut}$ studies. However, sustained depletion of CCR2^{+} cells is not feasible in human patients because of their critical role in immune defense. Thus, although CCR2^{+} monocytes represent a shared disease-driving population across desmosomal cardiomyopathy models, these findings suggest that precisely timed modulation of early inflammatory signaling, rather than global depletion of myeloid cells, is the more promising therapeutic strategy.

Currently, no approved disease-specific targeted therapy exists for ACM, and anti-inflammatory or immunosuppressive agents such as glucocorticoids (e.g., dexamethasone) and azathioprine are used only occasionally and off-label in symptomatic patients[5,55,56]. Such treatments are likely to be most beneficial when

516 applied during early or acute inflammatory disease phases, before irreversible
517 remodeling develops.

518 More targeted approaches, including IL-1β antagonists, have shown promising results
519 in related inflammatory cardiac conditions[57,58]. In *Pkp2*$^{+/-}$ mice, the therapeutic window
520 spans 9-12 months, whereas in patients, the optimal timing remains to be determined
521 and may vary between individuals. Our data align with retrospective clinical studies
522 suggesting that anti-inflammatory therapies could benefit desmoplakin mutation
523 carriers presenting with myocarditis-like symptoms[57,58]. Beyond therapeutic
524 modulation, our findings highlight the influence of secondary triggers on the course of
525 genetic cardiomyopathies. The absence of a cardiac phenotype following MCMV
526 infection in *Ttn*$^{+/-}$ mice suggests that the timing and sequence of second hits are critical
527 for disease manifestation. In humans, *TTN* variants are frequently detected in patients
528 with complicated myocarditis[7], which may reflect a scenario in which pre-existing,
529 subclinical myocardial impairment serves as a first hit that limits recovery after infection
530 and accelerates cardiomyopathy progression. In contrast, the viral challenge in our
531 mouse model, applied before structural changes developed, may have preceded this
532 window of susceptibility. It is conceivable that combining stressors, such as pregnancy,
533 alcohol abuse or toxic substances, with viral infection could unmask such vulnerability
534 in *Ttn*-deficient hearts[10]. In *Pkp2*-deficient hearts, however, latent MCMV proved to be
535 a potent trigger of cardiac dysfunction, a finding with direct translational relevance:
536 patients with PKP2 or other desmosomal mutations may particularly benefit from
537 avoiding physical exertion or promptly treating systemic infections. Preventive
538 measures, including vaccination and early antiviral therapy, should therefore be
539 applied for individuals with a genetic predisposition. Although no CMV vaccine is
540 currently available, antiviral agents such as ganciclovir, routinely used in

541 immunocompromised patients[59], could be explored as adjuncts to anti-inflammatory
542 treatment during early myocarditis-like episodes. In conclusion, our findings emphasize
543 infection control and timely immunomodulation as promising strategies to delay or
544 prevent disease progression in ACM.

545 This study also has limitations that should be considered when interpreting the results.
546 As with any mouse model, the immune and inflammatory responses characterized
547 here may not fully capture the complexity of human ACM, where genetic diversity,
548 lifelong antigen exposure and comorbidities shape disease expression. In addition,
549 only male mice were included in the MCMV-infected *Pkp2*$^{+/-}$ cohort, reflecting the
550 known male predominance in ACM, but future work should examine whether sex-
551 specific immune responses modify the disease trajectory. Our findings in *Ttn*$^{+/-}$ mice
552 represent a single truncating variant located in the A-band and therefore do not exclude
553 the possibility that other variants and location in titin and in particular additional
554 environmental triggers could interact with inflammation differently. Finally, while CCR2^{+}
555 monocytes emerged as a shared disease-driving population across desmosomal
556 cardiomyopathy models, their essential role in human host defense limits the direct
557 translational applicability of cell-depletion strategies.

558 Despite these considerations, the convergence of genetic, immunological, and
559 virological evidence across models provides strong support for early inflammatory
560 signaling as a central driver of desmosomal cardiomyopathy and highlights the
561 importance of defining clinically meaningful windows for therapeutic intervention.

7. Acknowledgements

The authors thank Anne Kilinç, Susanne Schraut and Daniela Urlaub for their dedicated technical assistance with mouse scoring, genotyping, and experimental procedures; Arnhild Grothey for providing the viral stocks; and Berkan Arslan for performing and analyzing echocardiographic measurements. Alicia Bender and Jakob Weilbach are acknowledged for their support during tissue collection, Sonja Luckhardt for expert technical assistance with cytokine profiling, and Alanis Barbosa Gulde for conducting the kinase activity analyses. We acknowledge the contributions of service projects PS1 and PS2 within the Collaborative Research Centre 1525 for their support in conducting echocardiography and supporting CITE-seq and single-cell transcriptomic profiling, respectively. Schematic subfigures were created in BioRender; Gerull, B. (2025) https://BioRender.com/hkmxgxg.

8. Sources of Funding

CC, GCR, SF, LD and BG received support from the German Research Foundation as part of the Collaborative Research Centre 1525 ‘Cardio-Immune Interfaces’ (grant number 453989101). BG received funding from the German Heart Foundation (Deutsche Herzstiftung e.V. ‘Plötzlicher Herztod’). MN was supported by the Otto Hess research fellowship of the German Cardiac Society (DGK). JK and SK received scholarships of the Graduate School of Life Science (GSLS), Würzburg.

9. Disclosures

None.

585 **10. Supplemental Material**

586 Supplemental Methods

587 Supplemental Figures

588 Supplemental Tables

589 References[11,30,44,60-78]

11. References

1. Schulz-Menger J, Collini V, Groschel J, Adler Y, Brucato A, Christian V, Ferreira VM, Gandjbakhch E, Heidecker B, Kerneis M, et al. 2025 ESC Guidelines for the management of myocarditis and pericarditis. *Eur Heart J*. 2025;46:3952–4041. doi: 10.1093/eurheartj/ehaf192
2. Bassetto G, Angriman F, Gava CPLD, Paldino A, Perotto M, Bordignon L, Gigli M, Ferro MD, Massa L, Altinier A, et al. Hot Phases Cardiomyopathy: Pathophysiology, Diagnostic Challenges, and Emerging Therapies. *Current Cardiology Reports*. 2025;27. doi: 10.1007/s11886-024-02168-6
3. Asatryan B, Asimaki A, Landstrom AP, Khanji MY, Odening KE, Cooper LT, Marchlinski FE, Gelzer AR, Semsarian C, Reichlin T, et al. Inflammation and Immune Response in Arrhythmogenic Cardiomyopathy: State-of-the-Art Review. *Circulation*. 2021;144:1646–1655. doi: 10.1161/CIRCULATIONAHA.121.055890
4. Gerull B, Heuser A, Wichter T, Paul M, Basson CT, McDermott DA, Lerman BB, Markowitz SM, Ellinor PT, MacRae CA, et al. Mutations in the desmosomal protein plakophilin-2 are common in arrhythmogenic right ventricular cardiomyopathy. *Nat Genet*. 2004;36:1162–1164. doi: 10.1038/ng1461
5. Peretto G, Barzaghi F, Cicalese MP, Di Resta C, Slavich M, Benedetti S, Giangiobbe S, Rizzo S, Palmisano A, Esposito A, et al. Immunosuppressive therapy in childhood-onset arrhythmogenic inflammatory cardiomyopathy. *Pacing and Clinical Electrophysiology*. 2021;44:552–556. doi: 10.1111/pace.14153
6. Martins D, Ovaert C, Khraiche D, Boddaert N, Bonnet D, Raimondi F. Myocardial inflammation detected by cardiac MRI in Arrhythmogenic right ventricular cardiomyopathy: A paediatric case series. *Int J Cardiol*. 2018;271:81–86. doi: 10.1016/j.ijcard.2018.05.116
7. Monda E, Bakalakos A, Cannie D, O'Mahony C, Syrris P, Kaski JP, Limongelli G, Elliott PM. Prevalence of Pathogenic Variants in Cardiomyopathy-Associated Genes in Acute Myocarditis: A Systematic Review and Meta-Analysis. *JACC Heart Fail*. 2024;12:1101–1111. doi: 10.1016/j.jchf.2024.02.012
8. Ammirati E, Raimondi F, Piriou N, Sardo Infirri L, Mohiddin SA, Mazzanti A, Shenoy C, Cavallari UA, Imazio M, Aquaro GD, et al. Acute Myocarditis Associated With Desmosomal Gene Variants. *JACC Heart Fail*. 2022;10:714–727. doi: 10.1016/j.jchf.2022.06.013
9. Gerull B, Gramlich M, Atherton J, McNabb M, Trombitas K, Sasse-Klaassen S, Seidman JG, Seidman C, Granzier H, Labeit S, et al. Mutations of TTN, encoding the giant muscle filament titin, cause familial dilated cardiomyopathy. *Nat Genet*. 2002;30:201–204. doi: 10.1038/ng815
10. Verdonschot JAJ, Heymans SRB. Dilated cardiomyopathy: second hits knock-down the heart. *European Heart Journal*. 2024;45:500–501. doi: 10.1093/eurheartj/ehad778
11. Gramlich M, Michely B, Krohne C, Heuser A, Erdmann B, Klaassen S, Hudson B, Magarin M, Kirchner F, Todiras M, et al. Stress-induced dilated cardiomyopathy in a knock-in mouse model mimicking human titin-based disease. *J Mol Cell Cardiol*. 2009;47:352–358. doi: 10.1016/j.yjmcc.2009.04.014
12. Kažukauskienė I, Baltrūnienė V, Jakubauskas A, Žurauskas E, Maneikienė VV, Daunoravičius D, Čelutkienė J, Ručinskas K, Grabauskienė V. Prevalence and prognostic relevance of myocardial inflammation and cardiotropic viruses in non-ischemic dilated cardiomyopathy. *Cardiology Journal*. 2022;29:441–453. doi: 10.5603/cj.a2020.0088
13. Wang H, Peng G, Bai J, He B, Huang K, Hu X, Liu D. Cytomegalovirus Infection and Relative Risk of Cardiovascular Disease (Ischemic Heart Disease, Stroke, and Cardiovascular Death): A Meta-Analysis of Prospective Studies Up to 2016. *J Am Heart Assoc*. 2017;6. doi: 10.1161/JAHA.116.005025

14. Spray L, McIntosh A, McCartney PJ, Macfarlane PW, Maznyczka A, Welsh P, Berry C, Spyridopoulos I. Latent Cytomegalovirus Infection Is Associated With Impaired Left Ventricular Function After ST-Segment–Elevation Myocardial Infarction. *Journal of the American Heart Association*. 2025;14. doi: 10.1161/jaha.124.040584
15. Bonavita CM, Cardin RD. Don't Go Breaking My Heart: MCMV as a Model for HCMV-Associated Cardiovascular Diseases. *Pathogens*. 2021;10:619. doi: 10.3390/pathogens10050619
16. Hoorntje ET, Te Rijdt WP, James CA, Pilichou K, Basso C, Judge DP, Bezzina CR, Van Tintelen JP. Arrhythmogenic cardiomyopathy: pathology, genetics, and concepts in pathogenesis. *Cardiovascular Research*. 2017;113:1521–1531. doi: 10.1093/cvr/cvx150
17. Chelko SP, Asimaki A, Andersen P, Bedja D, Amat-Alarcon N, Demazumder D, Jasti R, Macrae CA, Leber R, Kleber AG, et al. Central role for GSK3β in the pathogenesis of arrhythmogenic cardiomyopathy. *JCI Insight*. 2016;1. doi: 10.1172/jci.insight.85923
18. Ng KE, Delaney PJ, Thenet D, Murtough S, Webb CM, Zaman N, Tsisanova E, Mastroianni G, Walker SLM, Westaby JD, et al. Early inflammation precedes cardiac fibrosis and heart failure in desmoglein 2 murine model of arrhythmogenic cardiomyopathy. *Cell and Tissue Research*. 2021;386:79–98. doi: 10.1007/s00441-021-03488-7
19. Van Opbergen CJM, Noorman M, Pfenniger A, Copier JS, Vermij SH, Li Z, Van Der Nagel R, Zhang M, De Bakker JMT, Glass AM, et al. Plakophilin-2 Haploinsufficiency Causes Calcium Handling Deficits and Modulates the Cardiac Response Towards Stress. *International Journal of Molecular Sciences*. 2019;20:4076. doi: 10.3390/ijms20174076
20. Bubić I, Wagner M, Krmpotić A, Saulig T, Kim S, Yokoyama WM, Jonjić S, Koszinowski UH. Gain of Virulence Caused by Loss of a Gene in Murine Cytomegalovirus. *Journal of Virology*. 2004;78:7536–7544. doi: 10.1128/jvi.78.14.7536-7544.2004
21. Li Y, Xiao J, Li C, Yang M. Memory inflation: Beyond the acute phase of viral infection. *Cell Proliferation*. 2024;57. doi: 10.1111/cpr.13705
22. Yang S, Penna V, Lavine KJ. Functional diversity of cardiac macrophages in health and disease. *Nature Reviews Cardiology*. 2025;22:431–442. doi: 10.1038/s41569-024-01109-8
23. Deshmane SL, Kremlev S, Amini S, Sawaya BE. Monocyte chemoattractant protein-1 (MCP-1): an overview. *J Interferon Cytokine Res*. 2009;29:313–326. doi: 10.1089/jir.2008.0027
24. Huang L. The role of IL-17 family cytokines in cardiac fibrosis. *Frontiers in Cardiovascular Medicine*. 2024;11. doi: 10.3389/fcvm.2024.1470362
25. Lasrado N, Reddy J. An overview of the immune mechanisms of viral myocarditis. *Reviews in Medical Virology*. 2020;30:1–14. doi: 10.1002/rmv.2131
26. Alam F, Singh A, Flores-Malavet V, Sell S, Cooper AM, Swain SL, McKinstry KK, Strutt TM. CD25-Targeted IL-2 Signals Promote Improved Outcomes of Influenza Infection and Boost Memory CD4 T Cell Formation. *The Journal of Immunology*. 2020;204:3307–3314. doi: 10.4049/jimmunol.2000205
27. Ruan C-C, Kong L-R, Chen X-H, Ma Y, Pan X-X, Zhang Z-B, Gao P-J. A2A Receptor Activation Attenuates Hypertensive Cardiac Remodeling via Promoting Brown Adipose Tissue-Derived FGF21. *Cell Metabolism*. 2018;28:476–489.e475. doi: 10.1016/j.cmet.2018.06.013
28. Planavila A, Redondo-Angulo I, Ribas F, Garrabou G, Casademont J, Giralt M, Villarroya F. Fibroblast growth factor 21 protects the heart from oxidative stress. *Cardiovascular Research*. 2015;106:19–31. doi: 10.1093/cvr/cvu263
29. Gramlich M, Pane LS, Zhou Q, Chen Z, Murgia M, Schötterl S, Goedel A, Metzger K, Brade T, Parrotta E, et al. Antisense-mediated exon skipping: a therapeutic strategy for titin-based dilated cardiomyopathy. *EMBO Molecular Medicine*. 2015;7:562–576. doi: 10.15252/emmm.201505047

30. Dann E, Henderson NC, Teichmann SA, Morgan MD, Marioni JC. Differential abundance testing on single-cell data using k-nearest neighbor graphs. *Nat Biotechnol*. 2022;40:245–253. doi: 10.1038/s41587-021-01033-z
31. Ferrucci L, Fabbri E. Inflammageing: chronic inflammation in ageing, cardiovascular disease, and frailty. *Nature Reviews Cardiology*. 2018;15:505–522. doi: 10.1038/s41569-018-0064-2
32. Gong Q, Sharma M, Glass MC, Kuan EL, Chander A, Singh M, Graybuck LT, Thomson ZJ, LaFrance CM, Rachid Zaim S, et al. Multi-omic profiling reveals age-related immune dynamics in healthy adults. *Nature*. 2025. doi: 10.1038/s41586-025-09686-5
33. Zhang J, Tian M, Xia Z, Feng P. Roles of IκB kinase ε in the innate immune defense and beyond. *Virologica Sinica*. 2016;31:457–465. doi: 10.1007/s12250-016-3898-y
34. Storz P. Protein kinase D mediates a stress-induced NF-kappaB activation and survival pathway. *The EMBO Journal*. 2003;22:109–120. doi: 10.1093/emboj/cdg009
35. Ersahin T, Tuncbag N, Cetin-Atalay R. The PI3K/AKT/mTOR interactive pathway. *Molecular BioSystems*. 2015;11:1946–1954. doi: 10.1039/c5mb00101c
36. Brühl H, Cihak J, Plachý J, Kunz-Schughart L, Niedermeier M, Denzel A, Rodriguez Gomez M, Talke Y, Luckow B, Stangassinger M, et al. Targeting of Gr-1+,CCR2+ monocytes in collagen-induced arthritis. *Arthritis & Rheumatism*. 2007;56:2975–2985. doi: 10.1002/art.22854
37. Fowler K, Mucha J, Neumann M, Lewandowski W, Kaczanowska M, Grys M, Schmidt E, Natenshon A, Talarico C, Buck PO, et al. A systematic literature review of the global seroprevalence of cytomegalovirus: possible implications for treatment, screening, and vaccine development. *BMC Public Health*. 2022;22. doi: 10.1186/s12889-022-13971-7
38. Heald-Sargent TA, Forte E, Liu X, Thorp EB, Abecassis MM, Zhang ZJ, Hummel MA. New Insights Into the Molecular Mechanisms and Immune Control of Cytomegalovirus Reactivation. *Transplantation*. 2020;104:e118–e124. doi: 10.1097/TP.0000000000003138
39. Mitrović M, Arapović J, Jordan S, Fodil-Cornu N, Ebert S, Vidal SM, Krmpotić A, Reddehase MJ, Jonjić S. The NK Cell Response to Mouse Cytomegalovirus Infection Affects the Level and Kinetics of the Early CD8⁺T-Cell Response. *Journal of Virology*. 2012;86:2165–2175. doi: 10.1128/jvi.06042-11
40. Griessl M, Renzaho A, Freitag K, Seckert CK, Reddehase MJ, Lemmermann NAW. Stochastic Episodes of Latent Cytomegalovirus Transcription Drive CD8 T-Cell "Memory Inflation" and Avoid Immune Evasion. *Frontiers in Immunology*. 2021;12. doi: 10.3389/fimmu.2021.668885
41. Chen X, Peng Y, Ge S, Li Y. Inflammation and cardiac dysfunction during sepsis, muscular dystrophy, and myocarditis. *Burns & Trauma*. 2013;1:109. doi: 10.4103/2321-3868.123072
42. Asimaki A, Tandri H, Duffy ER, Winterfield JR, Mackey-Bojack S, Picken MM, Cooper LT, Wilber DJ, Marcus FI, Basso C, et al. Altered Desmosomal Proteins in Granulomatous Myocarditis and Potential Pathogenic Links to Arrhythmogenic Right Ventricular Cardiomyopathy. *Circulation: Arrhythmia and Electrophysiology*. 2011;4:743–752. doi: 10.1161/circep.111.964890
43. Lubos N, Van Der Gaag S, Gerçek M, Kant S, Leube RE, Krusche CA. Inflammation shapes pathogenesis of murine arrhythmogenic cardiomyopathy. *Basic Research in Cardiology*. 2020;115. doi: 10.1007/s00395-020-0803-5
44. Rizzo G, Gropper J, Piollet M, Vafadarnejad E, Rizakou A, Bandi SR, Arampatzi P, Krammer T, DiFabion N, Dietrich O, et al. Dynamics of monocyte-derived macrophage diversity in experimental myocardial infarction. *Cardiovasc Res*. 2023;119:772–785. doi: 10.1093/cvr/cvac113
45. Duan X, Zhang L, Liu K, Guo K, You Y, Jia H, Zhou S, Han B. Macrophage-derived SPP1 exacerbate myocardial injury by interacting with fibroblasts in viral myocarditis. *Biology Direct*. 2025;20. doi: 10.1186/s13062-025-00621-2

46. Feng G, Bajpai G, Ma P, Koenig A, Bredemeyer A, Lokshina I, Lai L, Forster I, Leuschner F, Kreisel D, et al. CCL17 Aggravates Myocardial Injury by Suppressing Recruitment of Regulatory T Cells. *Circulation*. 2022;145:765–782. doi: 10.1161/CIRCULATIONAHA.121.055888
47. Yousif LI, Tanja AA, De Boer RA, Teske AJ, Meijers WC. The role of immune checkpoints in cardiovascular disease. *Frontiers in Pharmacology*. 2022;13. doi: 10.3389/fphar.2022.989431
48. Deleon-Pennell KY, Iyer RP, Ero OK, Cates CA, Flynn ER, Cannon PL, Jung M, Shannon DA, Garrett MR, Buchanan W, et al. Periodontal-induced chronic inflammation triggers macrophage secretion of Ccl12 to inhibit fibroblast-mediated cardiac wound healing. *JCI Insight*. 2017;2. doi: 10.1172/jci.insight.94207
49. Baruzzi A, Iacobucci I, Soverini S, Lowell CA, Martinelli G, Berton G. c-Abl and Src-family kinases cross-talk in regulation of myeloid cell migration. *FEBS Lett*. 2010;584:15–21. doi: 10.1016/j.febslet.2009.11.009
50. Liang Y, Ye L. Bound to be perfect: Lck and T cell co-receptors. *Nature Immunology*. 2023;24:5–7. doi: 10.1038/s41590-022-01392-y
51. Parsons SA, Greer PA. The Fps/Fes kinase regulates the inflammatory response to endotoxin through down-regulation of TLR4, NF-κB activation, and TNF-α secretion in macrophages. *Journal of Leukocyte Biology*. 2006;80:1522–1528. doi: 10.1189/jlb.0506350
52. Chelko SP, Penna VR, Engel M, Shiel EA, Centner AM, Farra W, Cannon EN, Landim-Vieira M, Schaible N, Lavine K, et al. NFκB signaling drives myocardial injury via CCR2+ macrophages in a preclinical model of arrhythmogenic cardiomyopathy. *Journal of Clinical Investigation*. 2024;134. doi: 10.1172/jci172014
53. Pérez-Hernández M, Marrón-Liñares GM, Schlamp F, Heguy A, Van Opbergen CJM, Mezzano V, Zhang M, Liang F-X, Cerrone M, Delmar M. Transcriptomic Coupling of PKP2 With Inflammatory and Immune Pathways Endogenous to Adult Cardiac Myocytes. *Frontiers in Physiology*. 2021;11. doi: 10.3389/fphys.2020.623190
54. Nahrendorf M, Pittet MJ, Swirski FK. Monocytes: protagonists of infarct inflammation and repair after myocardial infarction. *Circulation*. 2010;121:2437–2445. doi: 10.1161/CIRCULATIONAHA.109.916346
55. Chimenti C, Russo MA, Frustaci A. Immunosuppressive therapy in virus-negative inflammatory cardiomyopathy: 20-year follow-up of the TIMIC trial. *Eur Heart J*. 2022;43:3463–3473. doi: 10.1093/eurheartj/ehac348
56. Gasperetti A, Muller SA, Peretto G, Asatryan B, Protonotarios A, Laredo M, Tarlet P-Y, Syrris P, Carrick RT, Murray B, et al. Prognostic Role of Myocarditis-Like Episodes and Their Treatment in Patients With Pathogenic Desmoplakin Variants. *Circulation*. 2025. doi: 10.1161/circulationaha.125.073919
57. Gasperetti A, Carrick RT, Muller S, Murray B, Adamo L, Bauce B, McNally E, Helms A. Desmoplakin Cardiomyopathy: Role of Inflammation and Potential Role of Disease-Modifying Therapies. *Current Cardiology Reports*. 2025;27. doi: 10.1007/s11886-024-02183-7
58. Lopez RI, Marchetta M, Ayers M, Mason P, Thomas M, Gasperetti A, Gilotra NA, Abbate A. Desmoplakin Cardiomyopathy Presenting With Recurrent Myopericarditis Responsive to Interleukin-1 Blockade. *JACC Case Rep*. 2025;30:104039. doi: 10.1016/j.jaccas.2025.104039
59. Kotton CN, Kamar N. New Insights on CMV Management in Solid Organ Transplant Patients: Prevention, Treatment, and Management of Resistant/Refractory Disease. *Infectious Diseases and Therapy*. 2023;12:333–342. doi: 10.1007/s40121-022-00746-1
60. Zinke R. A functional characterization of Plakophilin-2 and Desmoplakin in the adult mouse heart. . In; A functional characterization of Plakophilin–2 and Desmoplakin in the

adult mouse heart. Doctoral thesis, FU Berlin, Berlin, Germany. 2013; Retrieved from https://refubium.fu–berlin.de/handle/fub188/13779.

61. Puhl SL, Weeks KL, Ranieri A, Avkiran M. Assessing structural and functional responses of murine hearts to acute and sustained beta-adrenergic stimulation in vivo. *J Pharmacol Toxicol Methods*. 2016;79:60–71. doi: 10.1016/j.vascn.2016.01.007

62. Sacher T, Podlech J, Mohr CA, Jordan S, Ruzsics Z, Reddehase MJ, Koszinowski UH. The major virus-producing cell type during murine cytomegalovirus infection, the hepatocyte, is not the source of virus dissemination in the host. *Cell Host Microbe*. 2008;3:263–272. doi: 10.1016/j.chom.2008.02.014

63. Tischer BK, Smith GA, Osterrieder N. En passant mutagenesis: a two step markerless red recombination system. *Methods Mol Biol*. 2010;634:421–430. doi: 10.1007/978-1-60761-652-8_30

64. Brune W, Hengel H, Koszinowski UH. A mouse model for cytomegalovirus infection. *Curr Protoc Immunol*. 2001;Chapter 19:Unit 19 17. doi: 10.1002/0471142735.im1907s43

65. Mack M, Cihak J, Simonis C, Luckow B, Proudfoot AE, Plachy J, Bruhl H, Frink M, Anders HJ, Vielhauer V, et al. Expression and characterization of the chemokine receptors CCR2 and CCR5 in mice. *J Immunol*. 2001;166:4697–4704. doi: 10.4049/jimmunol.166.7.4697

66. Cardiff RD, Miller CH, Munn RJ. Manual hematoxylin and eosin staining of mouse tissue sections. *Cold Spring Harb Protoc*. 2014;2014:655–658. doi: 10.1101/pdb.prot073411

67. Rueden CT, Schindelin J, Hiner MC, DeZonia BE, Walter AE, Arena ET, Eliceiri KW. ImageJ2: ImageJ for the next generation of scientific image data. *BMC Bioinformatics*. 2017;18:529. doi: 10.1186/s12859-017-1934-z

68. Kammerer J, Cirnu A, Williams T, Hasselmeier M, Norpel M, Chen R, Gerull B. Macro-based collagen quantification and segmentation in picrosirius red-stained heart sections using light microscopy. *Biol Methods Protoc*. 2024;9:bpae027. doi: 10.1093/biomethods/bpae027

69. Zillikens H, Kasprick A, Osterloh C, Gross N, Radziewitz M, Hass C, Hartmann V, Behnen-Harer M, Ernst N, Boch K, et al. Topical Application of the PI3Kbeta-Selective Small Molecule Inhibitor TGX-221 Is an Effective Treatment Option for Experimental Epidermolysis Bullosa Acquisita. *Front Med (Lausanne)*. 2021;8:713312. doi: 10.3389/fmed.2021.713312

70. Szklarczyk D, Nastou K, Koutrouli M, Kirsch R, Mehryary F, Hachilif R, Hu D, Peluso ME, Huang Q, Fang T, et al. The STRING database in 2025: protein networks with directionality of regulation. *Nucleic Acids Res*. 2025;53:D730–D737. doi: 10.1093/nar/gkae1113

71. Metz KS, Deoudes EM, Berginski ME, Jimenez-Ruiz I, Aksoy BA, Hammerbacher J, Gomez SM, Phanstiel DH. Coral: Clear and Customizable Visualization of Human Kinome Data. *Cell Syst*. 2018;7:347–350 e341. doi: 10.1016/j.cels.2018.07.001

72. Team RC. R: A Language and Environment for Statistical Computing. https://www.R-project.org/. 2023.

73. Stoeckius M, Hafemeister C, Stephenson W, Houck-Loomis B, Chattopadhyay PK, Swerdlow H, Satija R, Smibert P. Simultaneous epitope and transcriptome measurement in single cells. *Nat Methods*. 2017;14:865–868. doi: 10.1038/nmeth.4380

74. Stoeckius M, Zheng S, Houck-Loomis B, Hao S, Yeung BZ, Mauck WM, 3rd, Smibert P, Satija R. Cell Hashing with barcoded antibodies enables multiplexing and doublet detection for single cell genomics. *Genome Biol*. 2018;19:224. doi: 10.1186/s13059-018-1603-1

75. Stuart T, Butler A, Hoffman P, Hafemeister C, Papalexi E, Mauck WM, 3rd, Hao Y, Stoeckius M, Smibert P, Satija R. Comprehensive Integration of Single-Cell Data. *Cell*. 2019;177:1888–1902 e1821. doi: 10.1016/j.cell.2019.05.031

76. McGinnis CS, Murrow LM, Gartner ZJ. DoubletFinder: Doublet Detection in Single-Cell RNA Sequencing Data Using Artificial Nearest Neighbors. *Cell Syst*. 2019;8:329–337 e324. doi: 10.1016/j.cels.2019.03.003

77. Korsunsky I, Millard N, Fan J, Slowikowski K, Zhang F, Wei K, Baglaenko Y, Brenner M, Loh PR, Raychaudhuri S. Fast, sensitive and accurate integration of single-cell data with Harmony. *Nat Methods*. 2019;16:1289–1296. doi: 10.1038/s41592-019-0619-0

78. Kuleshov MV, Jones MR, Rouillard AD, Fernandez NF, Duan Q, Wang Z, Koplev S, Jenkins SL, Jagodnik KM, Lachmann A, et al. Enrichr: a comprehensive gene set enrichment analysis web server 2016 update. *Nucleic Acids Res*. 2016;44:W90–97. doi: 10.1093/nar/gkw377

854 **12. Figures and Figure Legends**

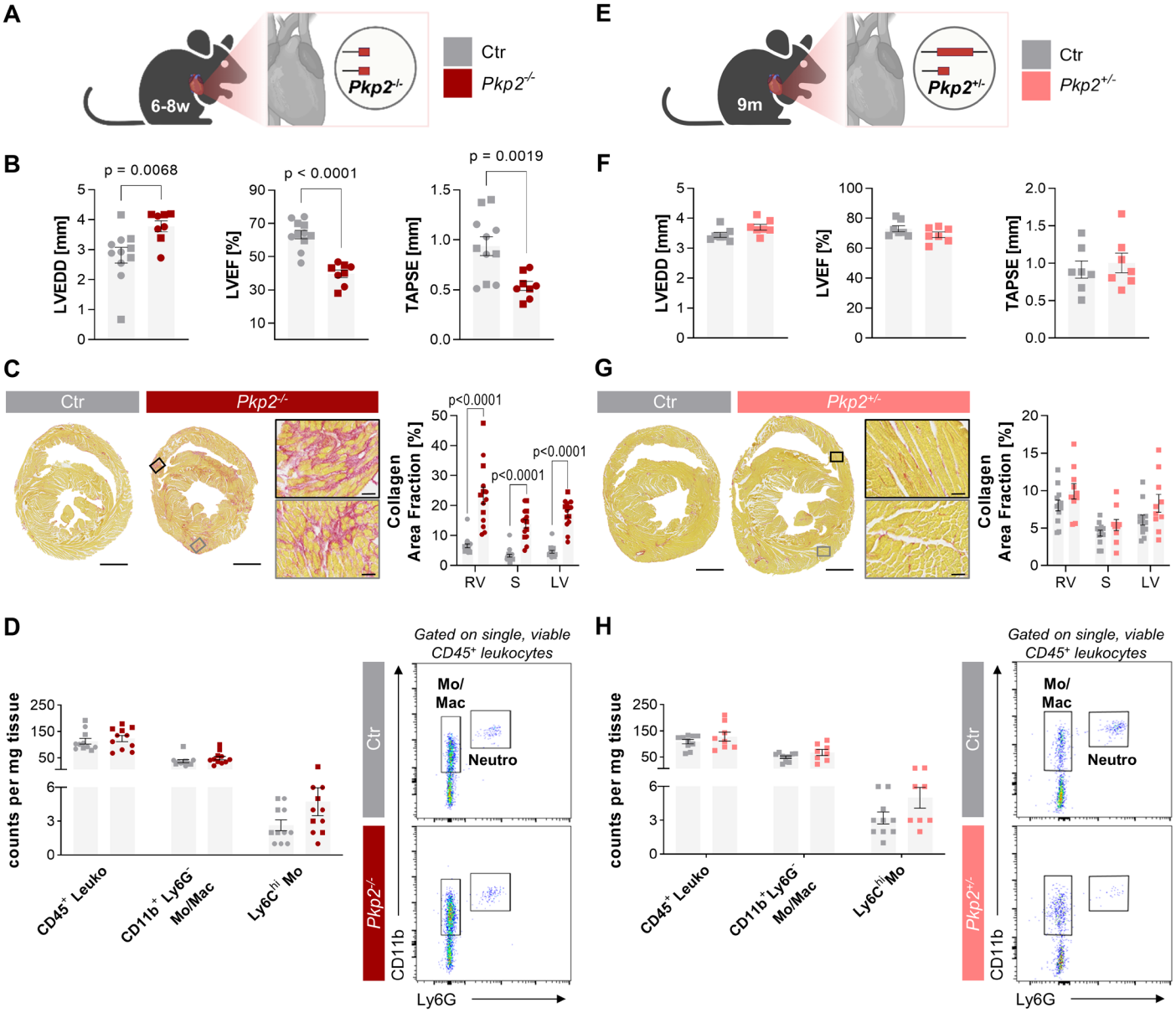

855 **Figure 1. Heterozygous *Pkp2* deficiency does not impact cardiac structure and**
856 **function, while homozygous loss of *Pkp2* leads to early cardiomyopathy.**

857 **A**, Scheme of homozygous cardiac-specific *Pkp2* knockout (*Pkp2*$^{-/-}$) mouse model;
858 signature colors: Ctr – grey, *Pkp2*$^{-/-}$ dark red. **B**, Quantification of echocardiographic
859 parameters at 6-8 weeks; Ctr n = 11, *Pkp2*$^{-/-}$ n = 8. **C**, Picrosirius red (PSR) stained
860 cardiac cross-sections and quantification of collagen area fraction; scale bars:
861 overview 1000µm, detail 50µm; Ctr n = 17, *Pkp2*$^{-/-}$ n = 14. **D**, Quantification of different
862 cardiac CD45^{+} leukocytes by flow cytometry in counts per milligram tissue;
863 representative dot plots showing monocytes/macrophages and neutrophils; Ctr n = 11,
864 *Pkp2*$^{-/-}$ n = 11. **E**, Scheme of heterozygous cardiac-specific *Pkp2* knockout (*Pkp2*$^{+/-}$)
865 mouse model; signature colors: Ctr – grey, *Pkp2*$^{+/-}$ pink. **F**, Quantification of
866 echocardiographic parameters at 9 months; Ctr n = 7, *Pkp2*$^{+/-}$ n = 7. **G**, PSR stained
867 cardiac cross-sections and quantification of collagen area fraction; scale bars:
868 overview 1000µm, detail 50µm; Ctr n = 12, *Pkp2*$^{+/-}$ n = 10. **H**, Quantification of different
869 cardiac CD45^{+} leukocytes by flow cytometry in counts per milligram tissue;
870 representative gating showing monocytes/macrophages and neutrophils; Ctr n = 10,
871 *Pkp2*$^{+/-}$ n = 8. Data as mean ± SEM. Male: squares; female: circles. Unpaired t test (±
872 Welch's correction) or Mann–Whitney test, as appropriate. Ctr – control, LVEDD – left
873 ventricular end-diastolic diameter, LVEF – left ventricular ejection fraction, TAPSE –
874 tricuspid annular plane systolic excursion, RV – right ventricle, S – septum, LV – left
875 ventricle, Leuko – leukocytes, Mo/Mac – monocytes/macrophages, Mo – monocytes,
876 Neutro – neutrophils.

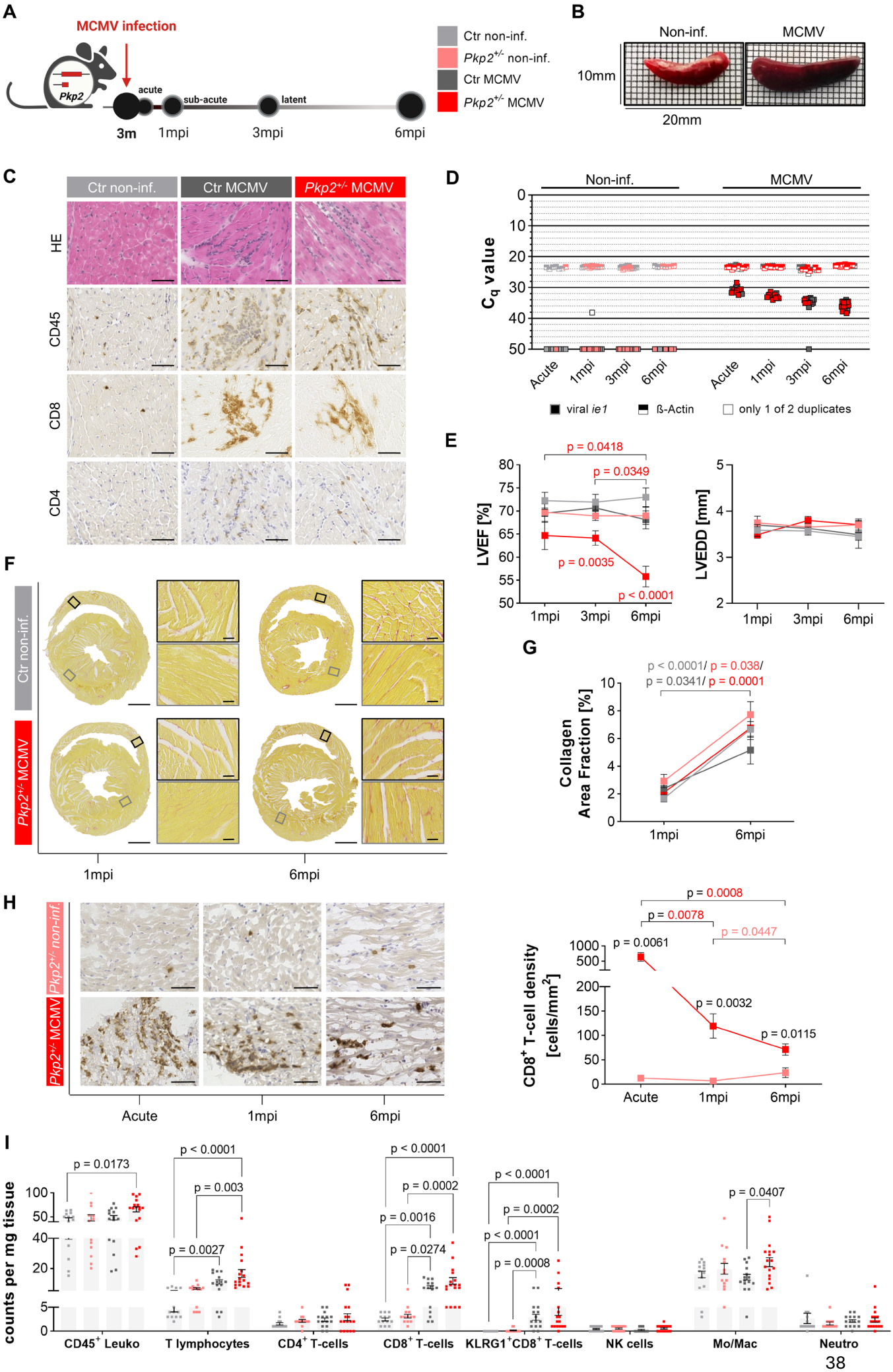
A
MCMV infection
Pkp2
acute
sub-acute
latent
3m
1mpi
3mpi
6mpi
Ctr non-inf.
Pkp2+/- non-inf.
Ctr MCMV
Pkp2+/- MCMV
B
Non-inf.
MCMV
10mm
20mm
C
Ctr non-inf.
Ctr MCMV
Pkp2+/- MCMV
HE
CD45
CD8
CD4
D
Non-inf.
MCMV
Cq value
Acute
1mpi
3mpi
6mpi
viral ie1
ß-Actin
only 1 of 2 duplicates
E
p = 0.0418
p = 0.0349
p = 0.0035
p < 0.0001
LVEF [%]
LVEDD [mm]
1mpi
3mpi
6mpi
F
Ctr non-inf.
Pkp2+/- MCMV
1mpi
6mpi
G
p < 0.0001/ p = 0.038/
p = 0.0341/ p = 0.0001
Collagen Area Fraction [%]
1mpi
6mpi
H
Pkp2+/- non-inf.
Pkp2+/- MCMV
Acute
1mpi
6mpi
p = 0.0008
p = 0.0078
p = 0.0447
p = 0.0061
p = 0.0032
p = 0.0115
CD8+ T-cell density [cells/mm2]
Acute
1mpi
6mpi
I
counts per mg tissue
p = 0.0173
p < 0.0001
p = 0.003
p = 0.0027
p < 0.0001
p = 0.0002
p = 0.0016
p = 0.0274
p < 0.0001
p = 0.0002
p < 0.0001
p = 0.0008
p = 0.0407
CD45+ Leuko
T lymphocytes
CD4+ T-cells
CD8+ T-cells
KLRG1+CD8+ T-cells
NK cells
Mo/Mac
Neutro

878 **Figure 2. MCMV infection accelerates functional cardiac abnormalities in**
879 **genetically predisposed *Pkp2*$^{+/-}$ mice.**

880 **A**, Schematic experimental design. 3-month-old *Pkp2*$^{+/-}$ and control (Ctr) mice were
881 infected with 5x10^5 plaque-forming units ∆m157-MCMV-eGFP (MCMV) or received
882 phosphate-buffered saline (PBS) and were analyzed at different time points post-
883 infection. Signature colors: Ctr non-infected (light grey), *Pkp2*$^{+/-}$ non-infected (light
884 pink), Ctr MCMV (dark grey) and *Pkp2*$^{+/-}$ MCMV (red). **B**, Splenomegaly was observed
885 in response to acute MCMV infection. **C**, Representative images of cardiac sections
886 stained with hematoxylin-eosin (HE) and antibodies against the surface markers CD45,
887 CD4 and CD8 during acute infection; scale bar 50µm. **D**, Viral *ie1* (*immediate early 1*,
888 filled squares) and murine ß-actin (half-top-filled squares) DNA copies detected by
889 quantitative polymerase-chain reaction in heart samples from acute to latent infection
890 represented by quantification cycle values (C_q). Measurements were performed in
891 technical duplicates. It is indicated by an unfilled symbol when only one value was
892 usable; n = Acute/1mpi/3mpi/6mpi: Ctr non-infected n = 6/6/6/4, *Pkp2*$^{+/-}$ non-infected n
893 = 1/7/8/4, Ctr MCMV n = 6/6/9/8, *Pkp2*$^{+/-}$ MCMV n = 8/9/6/13 (no statistics calculated).
894 **E**, Quantification of echocardiographic parameters from 1 to 6 months post-infection
895 (mpi); n = 1mpi/3mpi/6mpi: Ctr non-infected n = 6/9/7, *Pkp2*$^{+/-}$ non-infected n = 7/10/7,
896 Ctr MCMV n = 6/14/5, *Pkp2*$^{+/-}$ MCMV n = 8/13/7. **F+G**, Representative picrosirius red
897 staining of cardiac sections and quantification of collagen area fraction at 1 and 6mpi;
898 scale bars: overview 1000µm, detail 50µm; n = 1mpi/6mpi: Ctr non-infected n = 4/12,
899 *Pkp2*$^{+/-}$ non-infected n = 5/9, Ctr MCMV n = 2/10, *Pkp2*$^{+/-}$ MCMV n = 9/12. **H**,
900 Representative images of CD8$^+$ immunostaining and quantification of CD8$^+$ T-cell
901 density from acute to latent infection; scale bar 50µm; n = Acute/1mpi/3mpi/6mpi:
902 *Pkp2*$^{+/-}$ non-infected n = 4/6/11/9, *Pkp2*$^{+/-}$ MCMV n = 7/11/6/7. **I**, Flow cytometry
903 quantification of cardiac CD45$^+$ leukocytes in absolute counts per milligram tissue at
904 6mpi; Ctr non-infected n = 13, *Pkp2*$^{+/-}$ non-infected n = 13, Ctr MCMV n = 15, *Pkp2*$^{+/-}$
905 MCMV n = 17. Data are shown as mean ± SEM. Only male mice were used (square
906 symbol). Ordinary one-way ANOVA with or without Brown-Forsythe and Welch's
907 correction and Tukey's or Dunnett's T3 multiple comparisons, respectively or Kruskal-
908 Wallis test with Dunn's multiple comparisons, as appropriate for >2 groups. Unpaired t
909 test with or without Welch's correction or Mann-Whitney test, as appropriate for 2
910 groups. P-values in **E** are shown for one group over time (bracket) and across groups
911 at one time point compared to Ctr non-infected. All other p-values can be found in Table
912 S3-S6. m – months, LVEF – left ventricular ejection fraction, LVEDD left ventricular
913 end-diastolic diameter, NK cells – natural killer cells, Mo/Mac –
914 monocytes/macrophages.

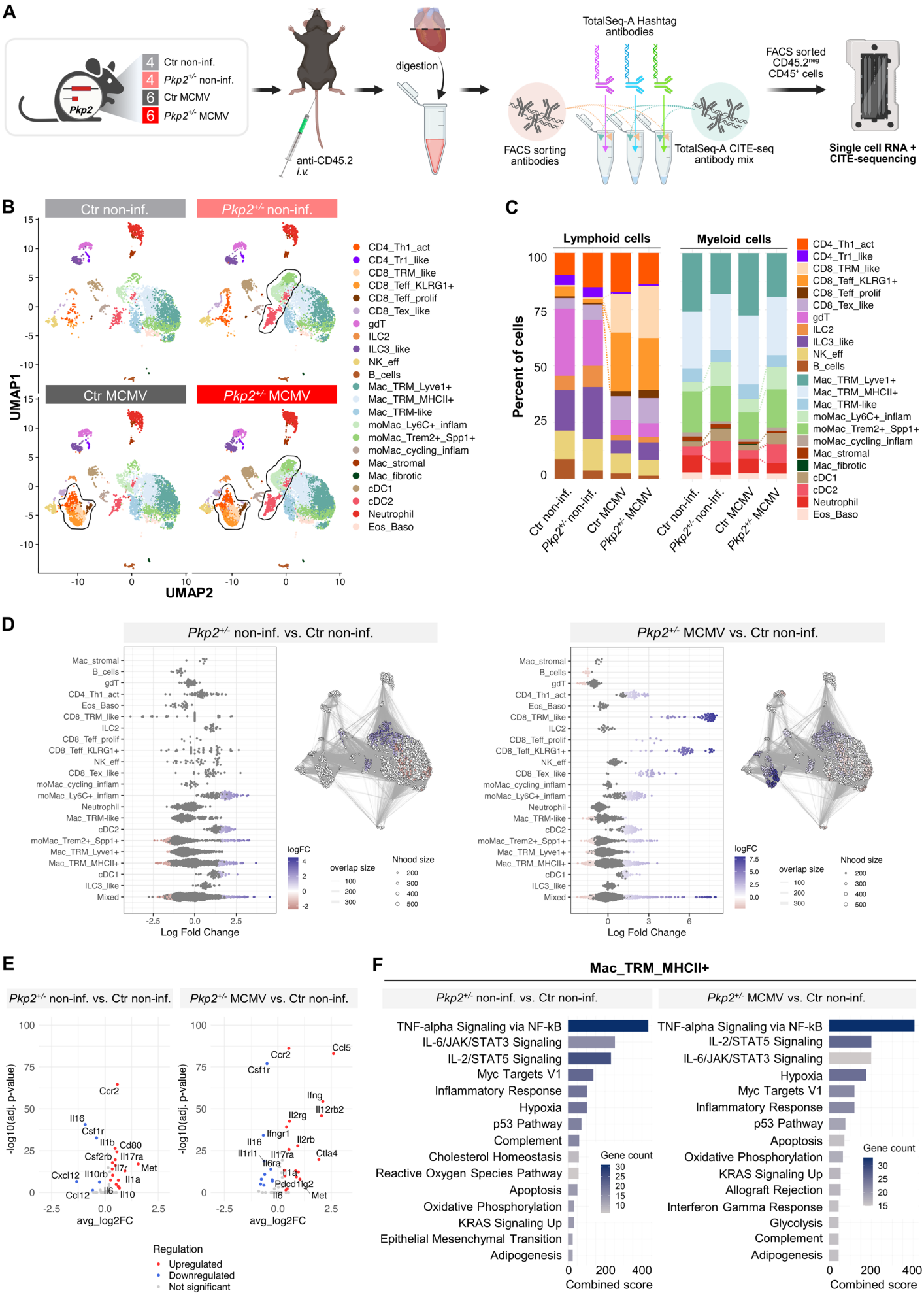
A
Pkp2
4 Ctr non-inf.
4 Pkp2+/- non-inf.
6 Ctr MCMV
6 Pkp2+/- MCMV
anti-CD45.2
i.v.
digestion
TotalSeq-A Hashtag antibodies
FACS sorting antibodies
TotalSeq-A CITE-seq antibody mix
FACS sorted CD45.2neg CD45+ cells
Single cell RNA + CITE-sequencing
B
Ctr non-inf.
Pkp2+/- non-inf.
Ctr MCMV
Pkp2+/- MCMV
UMAP1
UMAP2
CD4_Th1_act
CD4_Tr1_like
CD8_TRM_like
CD8_Teff_KLRG1+
CD8_Teff_prolif
CD8_Tex_like
gdT
ILC2
ILC3_like
NK_eff
B_cells
Mac_TRM_Lyve1+
Mac_TRM_MHCII+
Mac_TRM-like
moMac_Ly6C+_inflam
moMac_Trem2+_Spp1+
moMac_cycling_inflam
Mac_stromal
Mac_fibrotic
cDC1
cDC2
Neutrophil
Eos_Baso
C
Lymphoid cells
Myeloid cells
Percent of cells
Ctr non-inf.
Pkp2+/- non-inf.
Ctr MCMV
Pkp2+/- MCMV
D
Pkp2+/- non-inf. vs. Ctr non-inf.
Pkp2+/- MCMV vs. Ctr non-inf.
Log Fold Change
logFC
overlap size
Nhood size
E
Pkp2+/- non-inf. vs. Ctr non-inf.
Pkp2+/- MCMV vs. Ctr non-inf.
-log10(adj. p-value)
avg_log2FC
Ccr2
Il16
Csf1r
Il1b
Cd80
Csf2rb
Il17ra
Il7r
Met
Cxcl12
Il10rb
Il1a
Ccl12
Il6
Il10
Ccl5
Ifng
Il12rb2
Il2rg
Ifngr1
Il2rb
Il1r1
Il6ra
Ctla4
Pdcd1lg2
Regulation
Upregulated
Downregulated
Not significant
F
Mac_TRM_MHCII+
Pkp2+/- non-inf. vs. Ctr non-inf.
Pkp2+/- MCMV vs. Ctr non-inf.
TNF-alpha Signaling via NF-kB
IL-6/JAK/STAT3 Signaling
IL-2/STAT5 Signaling
Myc Targets V1
Inflammatory Response
Hypoxia
p53 Pathway
Complement
Cholesterol Homeostasis
Reactive Oxygen Species Pathway
Apoptosis
Oxidative Phosphorylation
KRAS Signaling Up
Epithelial Mesenchymal Transition
Adipogenesis
Gene count
Combined score

Figure 3. *Pkp2*$^{+/-}$ genotype is sufficient to induce subclinical accumulation of myeloid cell types before cardiac dysfunction emerges.

A, Schematic workflow of the CITE-seq experiment. At 6 months post-infection (mpi), mice received an intravenous (*i.v.*) injection of anti-CD45.2-APC before heart dissociation (ventricles only). Samples were multiplexed with TotalSeq-A hashtags and labeled with CITE-seq antibodies plus CD45 FACS antibody. Circulating cells were excluded by sorting CD45^{+} CD45.2-APC^{-} leukocytes. Two libraries from 10 pooled samples each were sequenced; Ctr non-infected n = 4, *Pkp2*$^{+/-}$ non-infected n = 4, Ctr MCMV n = 6, *Pkp2*$^{+/-}$ MCMV n = 6. **B**, UMAP representation of Seurat clustered leukocytes (in total 26,656) split by experimental group. **C**, Relative abundance of lymphoid and myeloid immune populations across groups. **D**, Assessment of statistically relevant changes in abundance using the MiloR package in *Pkp2*$^{+/-}$ non-infected and *Pkp2*$^{+/-}$ MCMV versus Ctr non-infected, respectively. **E**, Comparative cytokine expression analysis in cardiac leukocytes in *Pkp2*$^{+/-}$ non-infected and *Pkp2*$^{+/-}$ MCMV versus Ctr non-infected, respectively. **F**, Pathway enrichment analysis using MSig_DB_Hallmark_2020 database via the enrichR pipeline on pseudobulk-dataset. Shown are the top upregulated pathways by combined score in the subcluster Mac_TRM_MHCII+ of *Pkp2*$^{+/-}$ non-infected and *Pkp2*$^{+/-}$ MCMV versus Ctr non-infected, respectively. Ctr - control, CITE-seq - cellular indexing of transcriptomes and epitopes by sequencing, FACS – fluorescence-activated cell sorting, UMAP - uniform manifold approximation and projection.

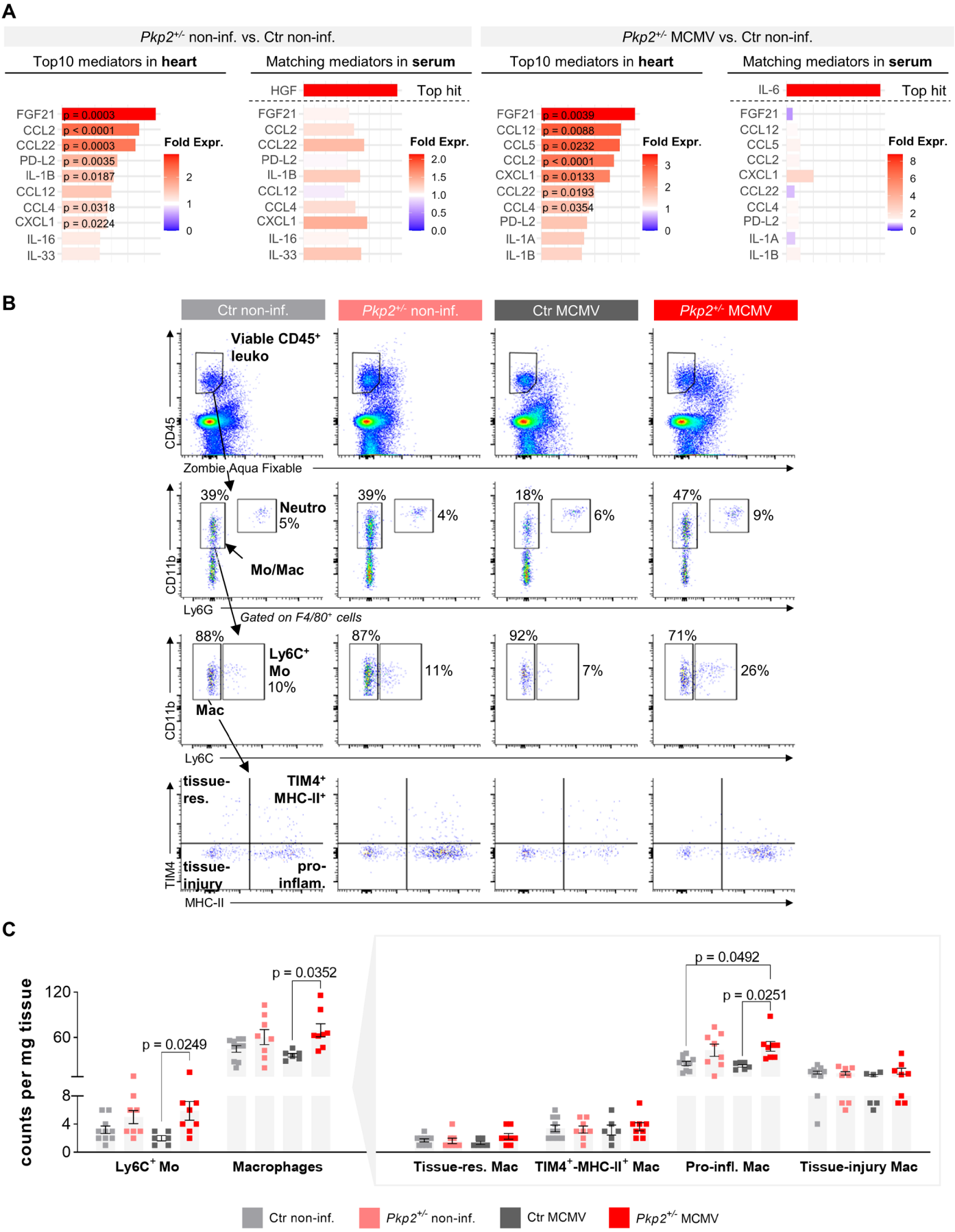
A
Pkp2+/- non-inf. vs. Ctr non-inf.
Top10 mediators in heart
FGF21 p = 0.0003
CCL2 p < 0.0001
CCL22 p = 0.0003
PD-L2 p = 0.0035
IL-1B p = 0.0187
CCL12
CCL4 p = 0.0318
CXCL1 p = 0.0224
IL-16
IL-33
Fold Expr.
Matching mediators in serum
HGF
Top hit
Pkp2+/- MCMV vs. Ctr non-inf.
Top10 mediators in heart
FGF21 p = 0.0039
CCL12 p = 0.0088
CCL5 p = 0.0232
CCL2 p < 0.0001
CXCL1 p = 0.0133
CCL22 p = 0.0193
CCL4 p = 0.0354
PD-L2
IL-1A
IL-1B
Matching mediators in serum
IL-6
Top hit
B
Ctr non-inf.
Pkp2+/- non-inf.
Ctr MCMV
Pkp2+/- MCMV
Viable CD45+ leuko
CD45
Zombie Aqua Fixable
39%
Neutro 5%
Mo/Mac
39%
4%
18%
6%
47%
9%
CD11b
Ly6G
Gated on F4/80+ cells
88%
Ly6C+ Mo 10%
Mac
87%
11%
92%
7%
71%
26%
Ly6C
tissue-res.
TIM4+ MHC-II+
tissue-injury
pro-inflam.
TIM4
MHC-II
C
counts per mg tissue
120
60
8
4
0
p = 0.0249
p = 0.0352
p = 0.0492
p = 0.0251
Ly6C+ Mo
Macrophages
Tissue-res. Mac
TIM4+-MHC-II+ Mac
Pro-infl. Mac
Tissue-injury Mac
Ctr non-inf.
Pkp2+/- non-inf.
Ctr MCMV
Pkp2+/- MCMV

938 **Figure 4. Heart-specific subclinical upregulation of cytokines in non-infected**
939 ***Pkp2*$^{+/-}$ mice.**

940 **A**, Cytokine profiling based on proximity extension assay at 6 months post-infection
941 (mpi). Shown are the top 10 differentially expressed heart mediators with
942 corresponding serum levels, plus the most altered serum-specific mediator. Expression
943 ratios compare *Pkp2*$^{+/-}$ non-infected and *Pkp2*$^{+/-}$ MCMV to Ctr non-infected,
944 respectively; n = heart/serum: Ctr non-infected n = 10/10, *Pkp2*$^{+/-}$ non-infected n =
945 10/10, Ctr MCMV n = 10/7, *Pkp2*$^{+/-}$ MCMV n = 10/8. **B+C**, Representative gating and
946 quantification of a myeloid-tailored flow cytometry panel of cardiac CD45^{+} leukocytes
947 from 6mpi hearts shown as absolute counts per milligram tissue; Ctr non-infected n =
948 10, *Pkp2*$^{+/-}$ non-infected n = 8, Ctr MCMV n = 6, *Pkp2*$^{+/-}$ MCMV n = 8. Data are shown
949 as mean ± SEM. Only male mice were used (square symbol). Unpaired t test with or
950 without Welch's correction or Mann-Whitney test, as appropriate for 2 groups. Ordinary
951 one-way ANOVA with or without Brown-Forsythe and Welch's correction and Tukey's
952 or Dunnett's T3 multiple comparisons, respectively or Kruskal-Wallis test with Dunn's
953 multiple comparisons, as appropriate for >2 groups. Ctr – control, Neutro – neutrophils,
954 Mo/Mac – monocytes/macrophages, Mo – monocytes, Mac – macrophages.

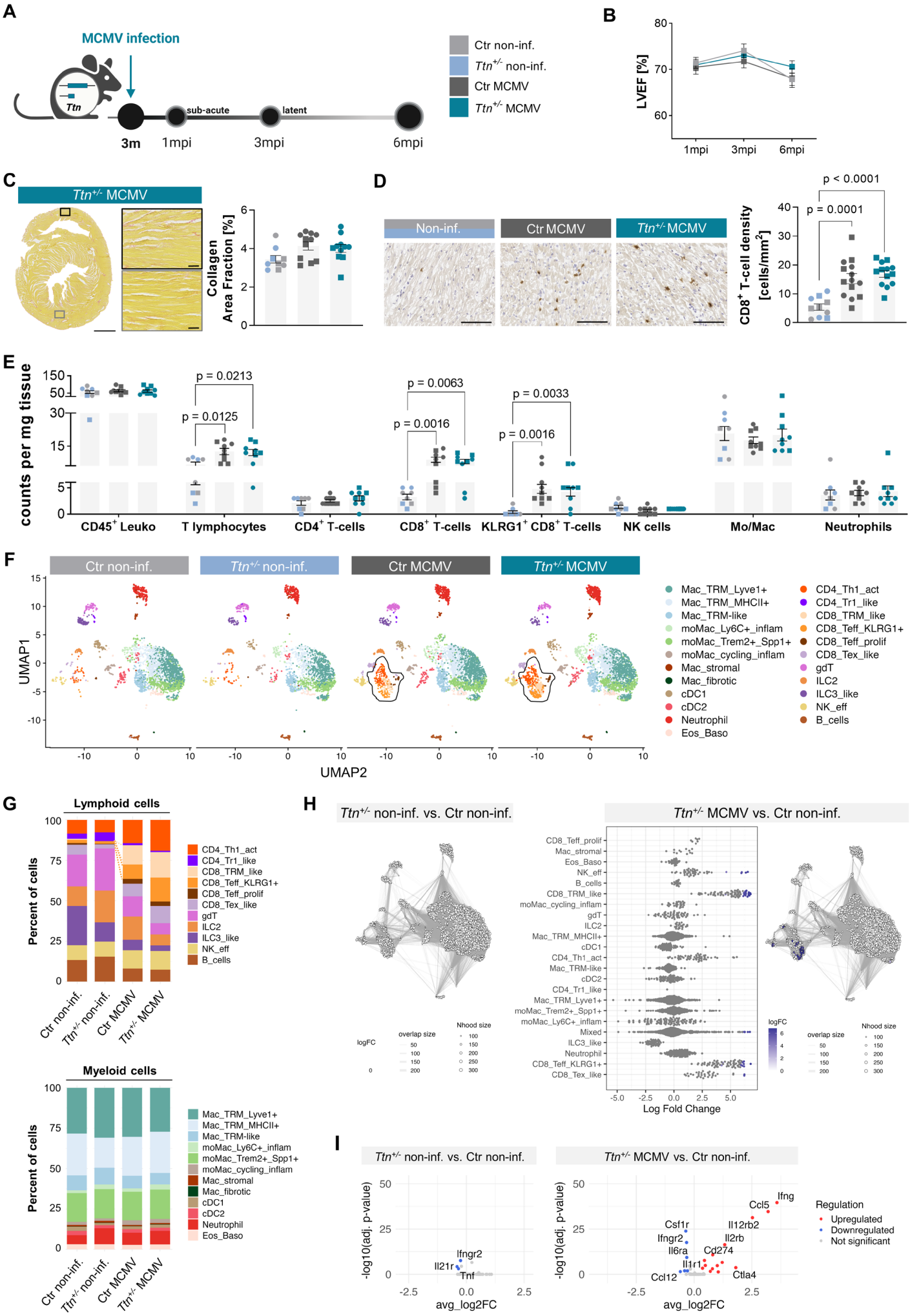
A
MCMV infection
Ttn
3m
1mpi
sub-acute
3mpi
latent
6mpi
Ctr non-inf.
Ttn+/- non-inf.
Ctr MCMV
Ttn+/- MCMV
B
LVEF [%]
80
70
60
1mpi
3mpi
6mpi
C
Ttn+/- MCMV
Collagen Area Fraction [%]
D
Non-inf.
Ctr MCMV
Ttn+/- MCMV
CD8+ T-cell density [cells/mm2]
p < 0.0001
p = 0.0001
E
counts per mg tissue
p = 0.0213
p = 0.0125
p = 0.0063
p = 0.0016
p = 0.0033
p = 0.0016
CD45+ Leuko
T lymphocytes
CD4+ T-cells
CD8+ T-cells
KLRG1+ CD8+ T-cells
NK cells
Mo/Mac
Neutrophils
F
Ctr non-inf.
Ttn+/- non-inf.
Ctr MCMV
Ttn+/- MCMV
UMAP1
UMAP2
Mac_TRM_Lyve1+
Mac_TRM_MHCII+
Mac_TRM-like
moMac_Ly6C+_inflam
moMac_Trem2+_Spp1+
moMac_cycling_inflam
Mac_stromal
Mac_fibrotic
cDC1
cDC2
Neutrophil
Eos_Baso
CD4_Th1_act
CD4_Tr1_like
CD8_TRM_like
CD8_Teff_KLRG1+
CD8_Teff_prolif
CD8_Tex_like
gdT
ILC2
ILC3_like
NK_eff
B_cells
G
Lymphoid cells
Percent of cells
Ctr non-inf.
Ttn+/- non-inf.
Ctr MCMV
Ttn+/- MCMV
Myeloid cells
H
Ttn+/- non-inf. vs. Ctr non-inf.
Ttn+/- MCMV vs. Ctr non-inf.
logFC
overlap size
Nhood size
Log Fold Change
I
Ttn+/- non-inf. vs. Ctr non-inf.
Ttn+/- MCMV vs. Ctr non-inf.
-log10(adj. p-value)
avg_log2FC
Ifngr2
Il21r
Tnf
Ifng
Ccl5
Csf1r
Il12rb2
Ifngr2
Il2rb
Il6ra
Cd274
Il1r1
Ccl12
Ctla4
Regulation
Upregulated
Downregulated
Not significant

Figure 5. MCMV does not trigger disease onset in a genetic mouse model of dilated cardiomyopathy with heterozygous loss of the sarcomeric gene *Ttn* (*Ttn*$^{+/-}$).

A, Schematic experimental design. 3-month-old *Ttn*$^{+/-}$ and control (Ctr) mice were infected with 5x10^5 plaque-forming units ∆m157-MCMV-eGFP (MCMV) or received phosphate-buffered saline (PBS) and were analyzed at different time points post-infection. Signature colors: Ctr non-infected (light grey), *Ttn*$^{+/-}$ non-infected (light blue), Ctr MCMV (dark grey) and *Ttn*$^{+/-}$ MCMV (blue). **B**, Left ventricular ejection fraction (LVEF) measured by echocardiography from 1 to 6 months post-infection (mpi); n = 1mpi/3mpi/6mpi: Ctr non-infected n = 5/5/4, *Ttn*$^{+/-}$ non-infected n = 5/5/5, Ctr MCMV n = 9/9/9, *Ttn*$^{+/-}$ MCMV n = 9/9/9. **C**, Representative picrosirius red stained *Ttn*$^{+/-}$ MCMV cardiac section and quantification of collagen area fraction at 6mpi; scale bars: overview 1000µm, detail 50 µm; Ctr non-infected + *Ttn*$^{+/-}$ non-infected n = 9, Ctr MCMV n = 11, *Ttn*$^{+/-}$ MCMV n = 11. **D**, Representative images of CD8$^+$ immunostaining in 6mpi heart sections and corresponding quantification of CD8$^+$ T-cell density; scale bar 50µm; Ctr non-infected + *Ttn*$^{+/-}$ non-infected n = 10, Ctr MCMV n = 14, *Ttn*$^{+/-}$ MCMV n = 13. **E**, Quantification of a lymphoid-tailored flow cytometry panel of cardiac CD45$^+$ leukocytes from 6mpi hearts shown as absolute counts per milligram tissue; Ctr non-infected + *Ttn*$^{+/-}$ non-infected n = 8, Ctr MCMV n = 9, *Ttn*$^{+/-}$ MCMV n = 9. **F**, UMAP representation of 12,660 cardiac leukocytes identified by CITE-seq split by experimental group at 6mpi; Ctr non-infected n = 2, *Ttn*$^{+/-}$ non-infected n = 2, Ctr MCMV n = 3, *Ttn*$^{+/-}$ MCMV n = 3. **G**, Relative cell type abundances across groups in lymphoid and myeloid cells at 6mpi. **H**, Assessment of statistically relevant changes in abundance using the MiloR package (p-value 0.1) in *Ttn*$^{+/-}$ non-infected and *Ttn*$^{+/-}$ MCMV versus Ctr non-infected, respectively. **I**, Comparative cytokine expression analysis in cardiac leukocytes (p-value 0.1) in *Ttn*$^{+/-}$ non-infected and *Ttn*$^{+/-}$ MCMV versus Ctr non-infected, respectively. Data are shown as mean ± SEM. Male: squares; female: circles. Ordinary one-way ANOVA with or without Brown-Forsythe and Welch's correction and Tukey's or Dunnett's T3 multiple comparisons, respectively or Kruskal-Wallis test with Dunn's multiple comparisons, as appropriate. Ctr – control, UMAP – uniform manifold approximation and projection, CITE-seq – cellular indexing of transcriptomes and epitopes by sequencing, NK cells – natural killer cells.

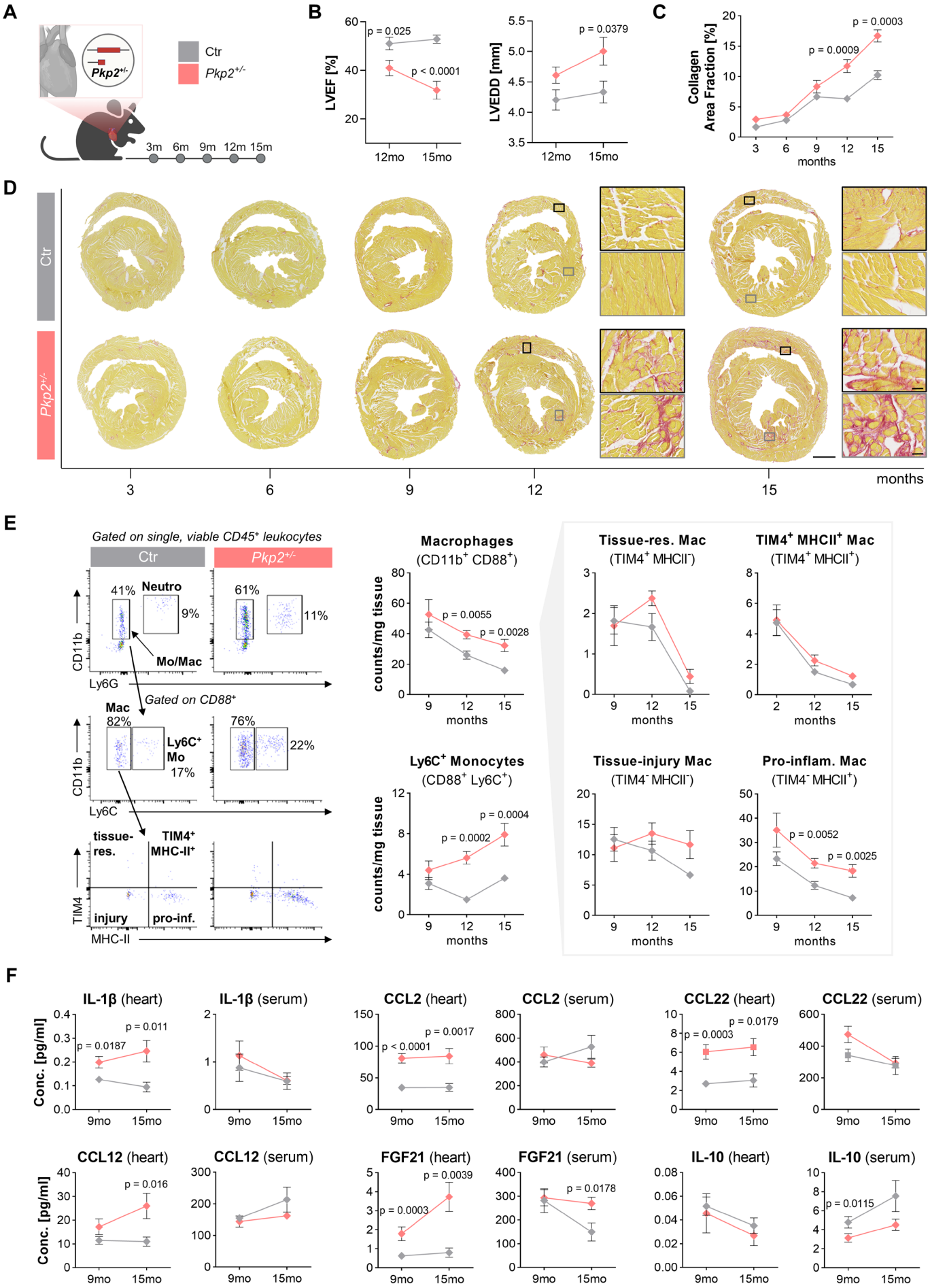
A
Pkp2+/-
Ctr
Pkp2+/-
3m 6m 9m 12m 15m
B
LVEF [%]
p = 0.025
p < 0.0001
12mo 15mo
LVEDD [mm]
p = 0.0379
12mo 15mo
C
Collagen Area Fraction [%]
p = 0.0003
p = 0.0009
months
D
Ctr
Pkp2+/-
3 6 9 12 15
months
E
Gated on single, viable CD45+ leukocytes
Ctr
Pkp2+/-
41% Neutro
9%
Mo/Mac
61%
11%
CD11b
Ly6G
Gated on CD88+
Mac 82%
Ly6C+ Mo 17%
76%
22%
Ly6C
tissue-res.
TIM4+ MHC-II+
injury
pro-inf.
TIM4
MHC-II
Macrophages (CD11b+ CD88+)
counts/mg tissue
p = 0.0055
p = 0.0028
months
Ly6C+ Monocytes (CD88+ Ly6C+)
p = 0.0004
p = 0.0002
Tissue-res. Mac (TIM4+ MHCII-)
TIM4+ MHCII+ Mac (TIM4+ MHCII+)
Tissue-injury Mac (TIM4- MHCII-)
Pro-inflam. Mac (TIM4- MHCII+)
p = 0.0052
p = 0.0025
F
IL-1β (heart)
p = 0.011
p = 0.0187
IL-1β (serum)
CCL2 (heart)
p = 0.0017
p < 0.0001
CCL2 (serum)
CCL22 (heart)
p = 0.0179
p = 0.0003
CCL22 (serum)
CCL12 (heart)
p = 0.016
CCL12 (serum)
FGF21 (heart)
p = 0.0039
p = 0.0003
FGF21 (serum)
p = 0.0178
IL-10 (heart)
IL-10 (serum)
p = 0.0115
Conc. [pg/ml]
9mo 15mo

Figure 6. Progressive development of a cardiac phenotype in aged *Pkp2*$^{+/-}$ mice.

A, Schematic overview of the experimental time points in *Pkp2*$^{+/-}$ and Ctr mice. **B**, Quantification of echocardiographic parameters at 12 and 15 months (mo); n = 12mo/15mo: Ctr n = 9/8, *Pkp2*$^{+/-}$ n = 9/9. **C+D**, Quantification of collagen area fraction and representative picrosirius red staining of cardiac sections from 3 to 15mo; scale bars: overview 1000µm, detail 50µm; n = 3mo/6mo/9mo/12mo/15mo: Ctr n = 4/7/12/6/7, *Pkp2*$^{+/-}$ n = 5/6/10/8/10. **E**, Representative gating and quantification of different cardiac CD45^{+} leukocytes at 9, 12 and 15mo by flow cytometry in counts per milligram tissue; n = 9mo/12mo/15mo: Ctr n = 11/6/12, *Pkp2*$^{+/-}$ n = 10/8/10. **F**, Cytokine profiling based on proximity extension assay at 9 and 15mo; n = 9mo/15mo: Ctr n = 10/6, *Pkp2*$^{+/-}$ n = 10/10. Data are shown as mean ± SEM. Unpaired t test with or without Welch's correction or Mann-Whitney test, as appropriate for 2 groups. Ordinary one-way ANOVA with or without Brown-Forsythe and Welch's correction and Tukey's or Dunnett's T3 multiple comparisons, respectively or Kruskal-Wallis test with Dunn's multiple comparisons, as appropriate for >2 groups. P-values for comparisons between groups at a given time point are shown in the graph; p-values for longitudinal comparisons within groups are provided in Table S14-S17. Ctr – control, LVEF – left ventricular ejection fraction, LVEDD – left ventricular end-diastolic diameter, Neutro – neutrophils, Mo/Mac – monocytes/macrophages, Mo – monocytes, Mac – macrophages.

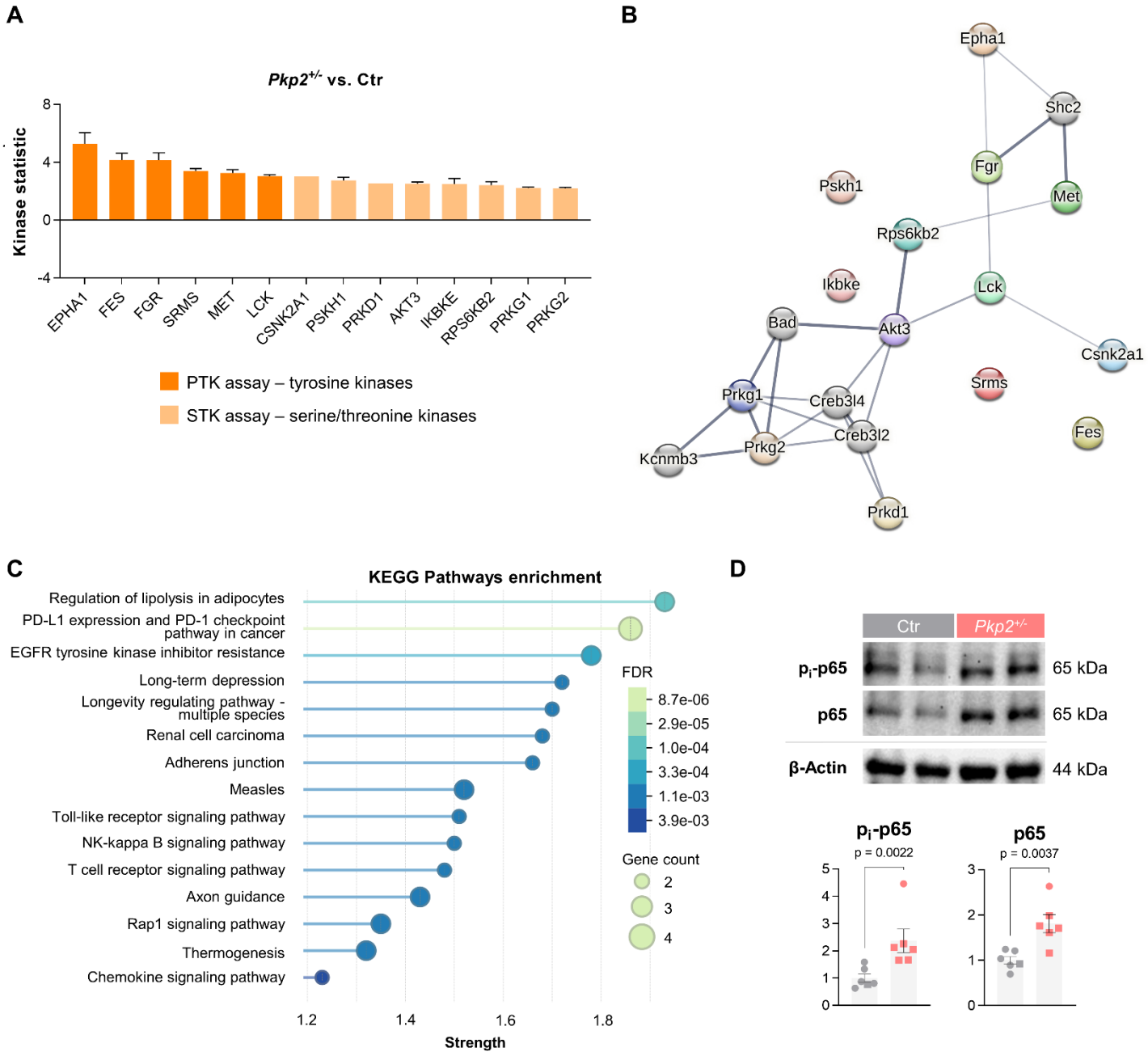
A
Pkp2+/- vs. Ctr
Kinase statistic
8
4
0
-4
EPHA1
FES
FGR
SRMS
MET
LCK
CSNK2A1
PSKH1
PRKD1
AKT3
IKBKE
RPS6KB2
PRKG1
PRKG2
PTK assay – tyrosine kinases
STK assay – serine/threonine kinases
B
Epha1
Shc2
Fgr
Met
Pskh1
Rps6kb2
Ikbke
Lck
Bad
Akt3
Csnk2a1
Srms
Prkg1
Creb3l4
Creb3l2
Fes
Prkg2
Kcnmb3
Prkd1
C
KEGG Pathways enrichment
Regulation of lipolysis in adipocytes
PD-L1 expression and PD-1 checkpoint pathway in cancer
EGFR tyrosine kinase inhibitor resistance
Long-term depression
Longevity regulating pathway - multiple species
Renal cell carcinoma
Adherens junction
Measles
Toll-like receptor signaling pathway
NK-kappa B signaling pathway
T cell receptor signaling pathway
Axon guidance
Rap1 signaling pathway
Thermogenesis
Chemokine signaling pathway
1.2
1.4
1.6
1.8
Strength
FDR
8.7e-06
2.9e-05
1.0e-04
3.3e-04
1.1e-03
3.9e-03
Gene count
2
3
4
D
Ctr
Pkp2+/-
pi-p65
65 kDa
p65
65 kDa
β-Actin
44 kDa
pi-p65
p = 0.0022
p65
p = 0.0037

1010 **Figure 7. Activation of inflammatory and compensatory signaling in *Pkp2*$^{+/-}$**
1011 **hearts at 12 months.**

1012 **A**, Comparative PamChip kinome profiling of *Pkp2*$^{+/-}$ hearts versus Ctr hearts at 12
1013 months; Ctr n = 4, *Pkp2*$^{+/-}$ n = 3. Bar plot representation of altered tyrosine (PTK) and
1014 serine/threonine (STK) kinases ranked by mean kinase statistic; Ctr n = 4, *Pkp2*$^{+/-}$ n =
1015 3. **B**, STRING interactions at medium confidence level. Line thickness correlates with
1016 predicted interaction strength. **C**, KEGG pathway enrichment of identified signaling
1017 networks. **D**, Western blot quantification and representative blot snips of
1018 phosphorylated p65 (p_i-p65, Ser536) and p65 protein levels in 15-month-old hearts
1019 normalized to β-Actin levels; Ctr n = 6, *Pkp2*$^{+/-}$ n = 6. Data are shown as mean ± SEM.
1020 Male: squares; female: circles. Unpaired t test with or without Welch's correction or
1021 Mann-Whitney test, as appropriate. Ctr – control, KEGG – Kyoto Encyclopedia of
1022 Genes and Genomes.

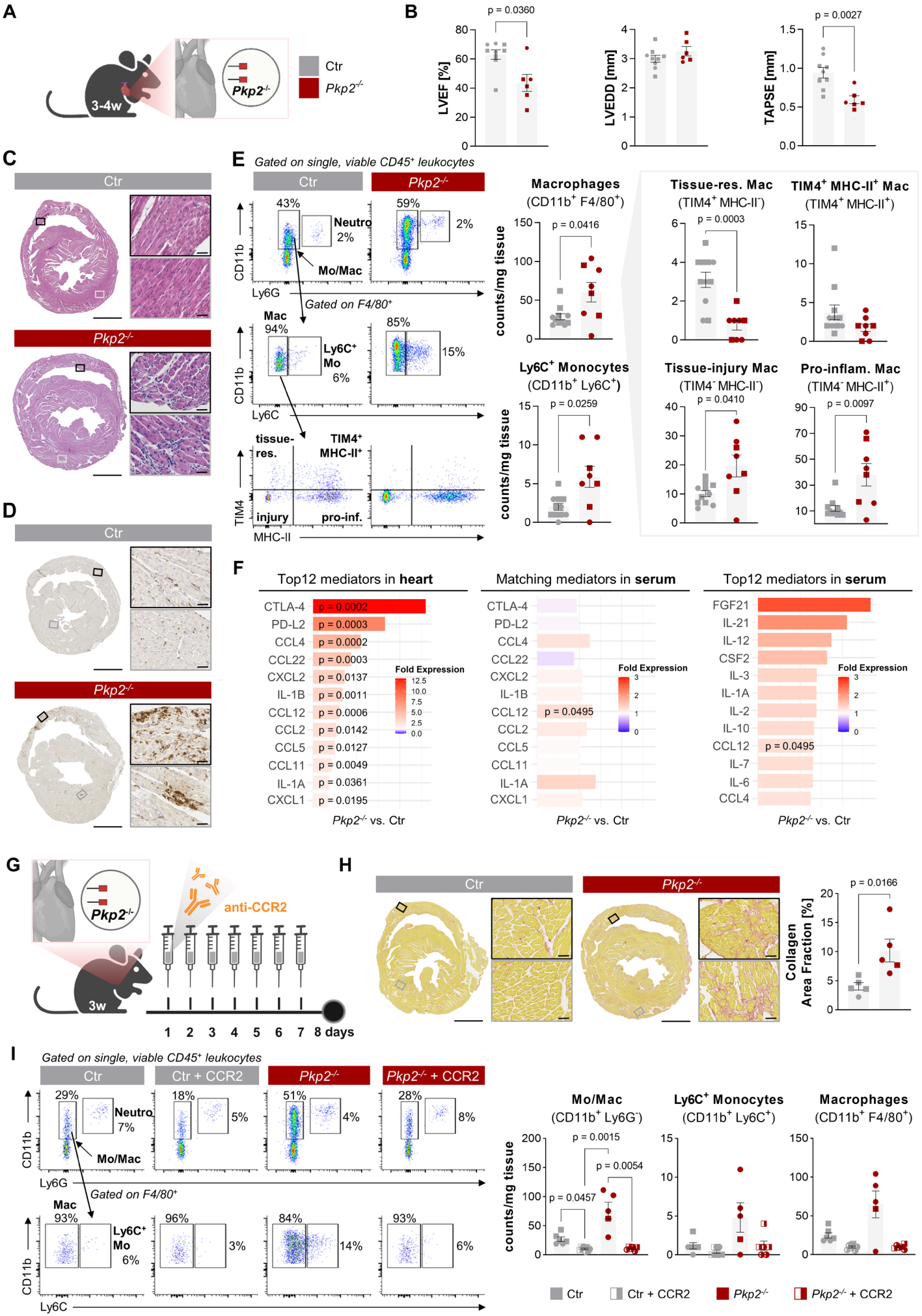
A
3-4w
Pkp2-/-
Ctr
Pkp2-/-
B
p = 0.0360
LVEF [%]
LVEDD [mm]
p = 0.0027
TAPSE [mm]
C
Ctr
Pkp2-/-
D
Ctr
Pkp2-/-
E
Gated on single, viable CD45+ leukocytes
Ctr
Pkp2-/-
43%
Neutro
2%
Mo/Mac
59%
2%
CD11b
Ly6G
Gated on F4/80+
Mac
94%
Ly6C+
Mo
6%
85%
15%
Ly6C
tissue-
res.
TIM4+
MHC-II+
injury
pro-inf.
TIM4
MHC-II
Macrophages
(CD11b+ F4/80+)
p = 0.0416
counts/mg tissue
Tissue-res. Mac
(TIM4+ MHC-II-)
p = 0.0003
TIM4+ MHC-II+ Mac
(TIM4+ MHC-II+)
Ly6C+ Monocytes
(CD11b+ Ly6C+)
p = 0.0259
Tissue-injury Mac
(TIM4- MHC-II-)
p = 0.0410
Pro-inflam. Mac
(TIM4- MHC-II+)
p = 0.0097
F
Top12 mediators in heart
CTLA-4 p = 0.0002
PD-L2 p = 0.0003
CCL4 p = 0.0002
CCL22 p = 0.0003
CXCL2 p = 0.0137
IL-1B p = 0.0011
CCL12 p = 0.0006
CCL2 p = 0.0142
CCL5 p = 0.0127
CCL11 p = 0.0049
IL-1A p = 0.0361
CXCL1 p = 0.0195
Fold Expression
Pkp2-/- vs. Ctr
Matching mediators in serum
CTLA-4
PD-L2
CCL4
CCL22
CXCL2
IL-1B
CCL12 p = 0.0495
CCL2
CCL5
CCL11
IL-1A
CXCL1
Pkp2-/- vs. Ctr
Top12 mediators in serum
FGF21
IL-21
IL-12
CSF2
IL-3
IL-1A
IL-2
IL-10
CCL12 p = 0.0495
IL-7
IL-6
CCL4
Pkp2-/- vs. Ctr
G
Pkp2-/-
3w
anti-CCR2
1 2 3 4 5 6 7 8 days
H
Ctr
Pkp2-/-
p = 0.0166
Collagen
Area Fraction [%]
I
Gated on single, viable CD45+ leukocytes
Ctr
Ctr + CCR2
Pkp2-/-
Pkp2-/- + CCR2
29%
Neutro
7%
Mo/Mac
18%
5%
51%
4%
28%
8%
Gated on F4/80+
Mac
93%
Ly6C+
Mo
6%
96%
3%
84%
14%
93%
6%
Mo/Mac
(CD11b+ Ly6G-)
p = 0.0015
p = 0.0054
p = 0.0457
Ly6C+ Monocytes
(CD11b+ Ly6C+)
Macrophages
(CD11b+ F4/80+)
counts/mg tissue
Ctr
Ctr + CCR2
Pkp2-/-
Pkp2-/- + CCR2

Figure 8 Anti-CCR2 intervention reduced numbers of recruited inflammatory monocytes and macrophages in more severely affected homozygous *Pkp2*$^{-/-}$ mice.

A, Schematic representation of homozygous cardiac-specific *Pkp2* knockout (*Pkp2*$^{-/-}$) mice at 3-4 weeks of age; signature colors: Ctr - grey, *Pkp2*$^{-/-}$ - dark red. **B**, Quantification of echocardiographic parameters at 3-4 weeks; Ctr n = 9, *Pkp2*$^{-/-}$ n = 6. **C**, Representative images of cardiac sections stained with hematoxylin-eosin (HE); scale bars: overview 1000µm, detail 50µm. **D**, Representative images of cardiac immunostaining against the macrophage surface marker CD68; scale bars: overview 1000µm, detail 50µm. **E**, Representative gating and quantification of different cardiac CD45^{+} leukocytes at 3-4 weeks by flow cytometry, shown in counts per milligram tissue; Ctr n = 11, *Pkp2*$^{-/-}$ n = 8. **F**, Cytokine profiling based on proximity extension assay at 3-4 weeks comparing expression ratios of *Pkp2*$^{-/-}$ versus Ctr heart and serum samples. Shown are the top 12 differentially expressed heart mediators with corresponding serum levels along with the top 12 most altered serum-specific mediators; n = heart/serum: Ctr n = 10/10, *Pkp2*$^{-/-}$ n = 10/10. **G**, Schematic representation of anti-CCR2 antibody treatment of *Pkp2*$^{-/-}$ and Ctr mice at 3 weeks of age. **H**, Representative picrosirius red staining of cardiac sections and quantification of collagen area fraction without anti-CCR2 treatment; scale bars: overview 1000µm, detail 50µm; Ctr n = 5, *Pkp2*$^{-/-}$ n = 5. **I**, Representative flow cytometry gating and quantification of different cardiac CD45^{+} leukocytes following anti-CCR2 treatment represented in counts per milligram tissue; untreated – filled symbol, anti-CCR2 treated – half-filled symbol; Ctr n = 6, Ctr+CCR2 n = 8, *Pkp2*$^{-/-}$ n = 5, *Pkp2*$^{-/-}$+CCR2 n = 6. Data are shown as mean ± SEM. Male: squares; female: circles. Unpaired t test with or without Welch's correction or Mann-Whitney test, as appropriate for 2 groups. Ordinary one-way ANOVA with or without Brown-Forsythe and Welch's correction and Tukey's or Dunnett's T3 multiple comparisons, respectively or Kruskal-Wallis test with Dunn's multiple comparisons, as appropriate for >2 groups. w – weeks, Ctr – control, LVEF – left ventricular ejection fraction, LVEDD – left ventricular end-diastolic diameter, TAPSE – tricuspid annular plane systolic excursion, Neutro – neutrophils, Mo/Mac – monocytes/macrophages, Mo – monocytes, Mac – macrophages.